Electronic Supplementary Material (ESI) for Dalton Transactions.

Electronic Supporting Information

1,4-Dihydropyridyl Complexes of Magnesium: Synthesis by Pyridine Insertion into the Magnesium-Silicon Bond of Triphenylsilyls and Catalytic Pyridine Hydrofunctionalization

L. E. Lemmerz,[a] T. P. Spaniol[a] and J. Okuda[a]*

Institute of Inorganic Chemistry, RWTH Aachen University, Landoltweg 1, 52056 Aachen, Germany

Table of Contents

1. ^{1}H, $^{13}C\{^{1}H\}$ and $^{29}Si\{^{1}H\}$ NMR spectra of $[Mg(NC_5H_5\text{-}4\text{-}SiPh_3)_2(THF)_3]$ (2)

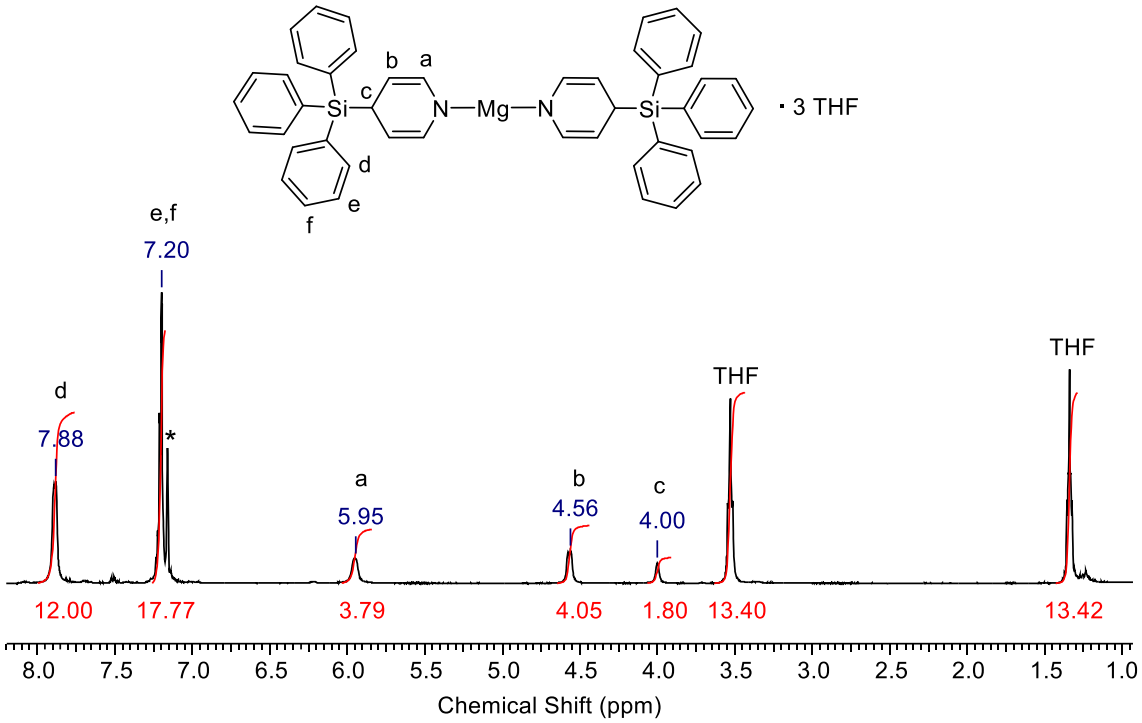

Figure S1. ^{1}H NMR spectrum of **2** in benzene-d_6 (*) at 25 °C.

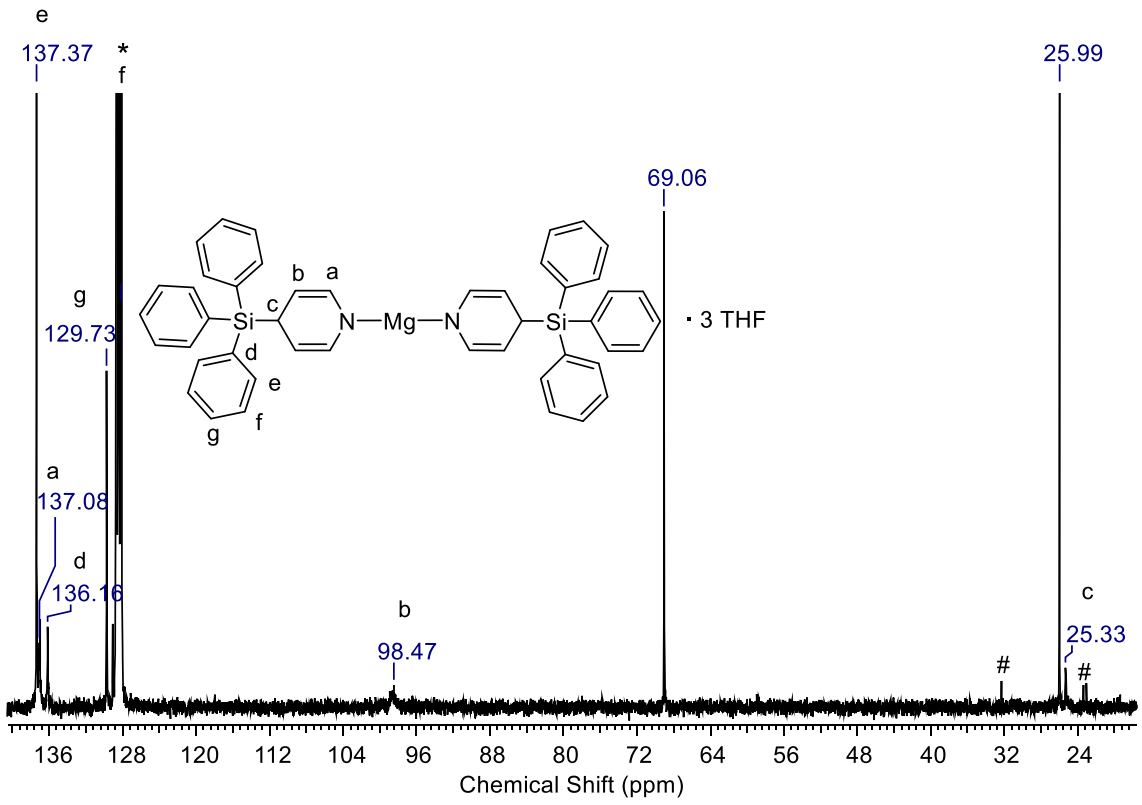

Figure S2. $^{13}C\{^{1}H\}$ NMR spectrum of **2** in benzene-d_6 (*) at 25 °C. (# unidentified species)

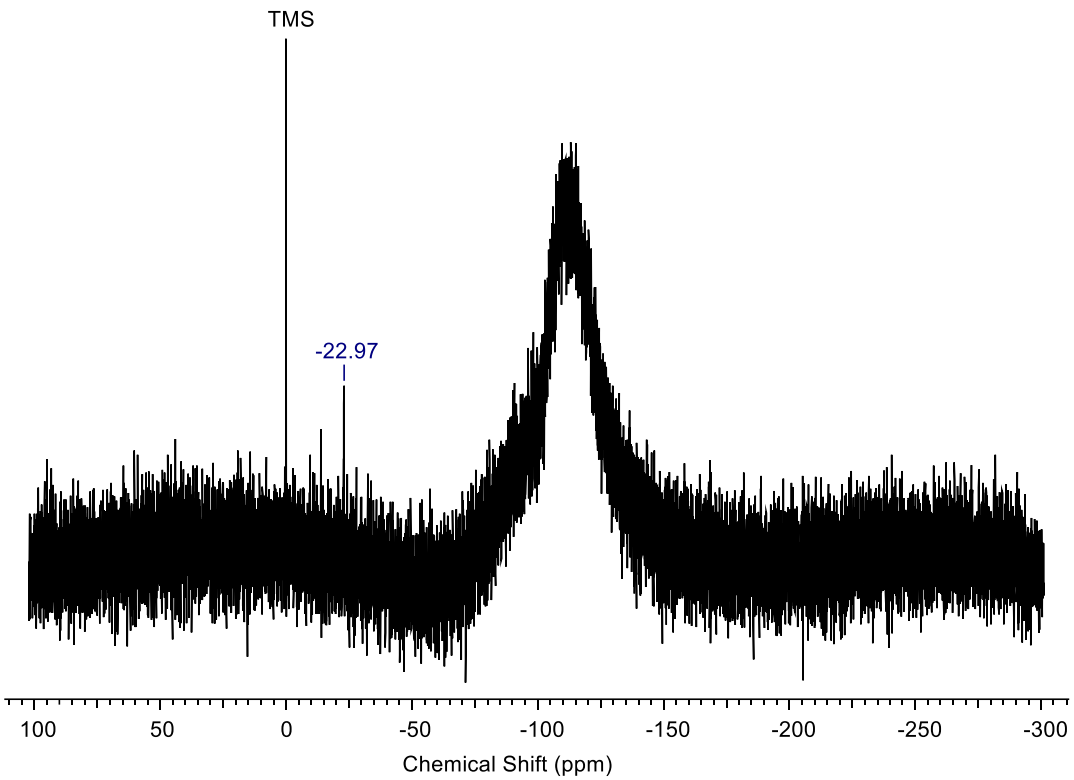

Figure S3. $^{29}Si\{^{1}H\}$ NMR spectrum of **2** in benzene-d_6 at 25 °C.

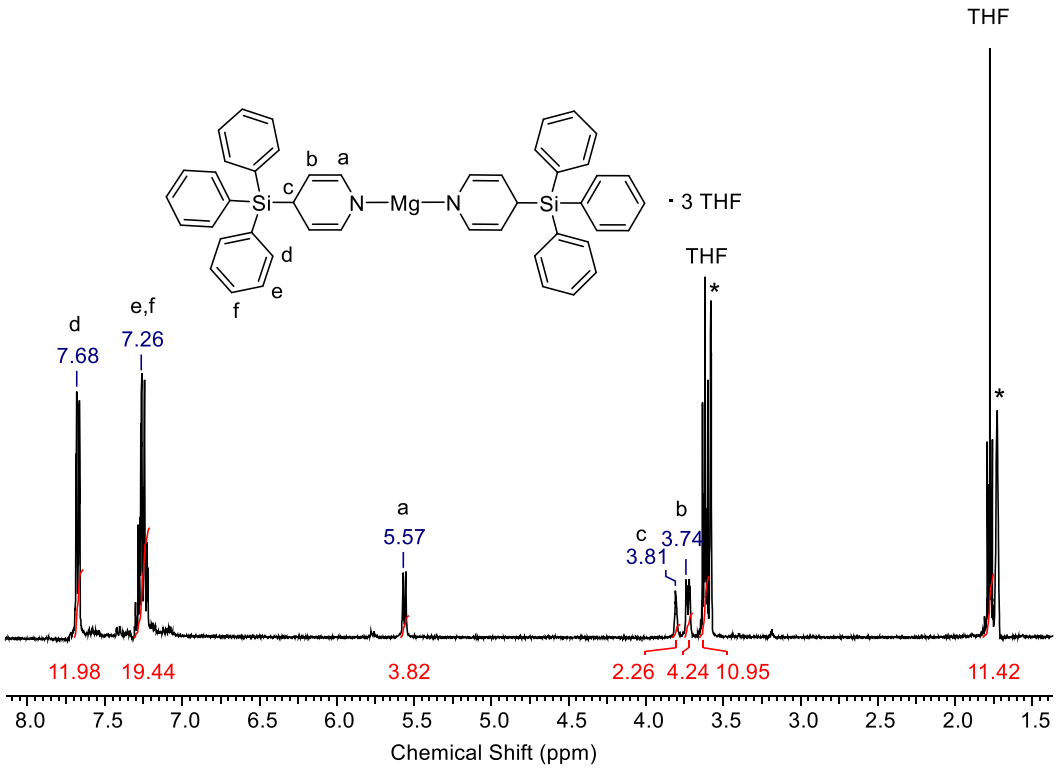

Figure S4. ^{1}H NMR spectrum of **2** in THF-d_8 (*) at 25 °C.

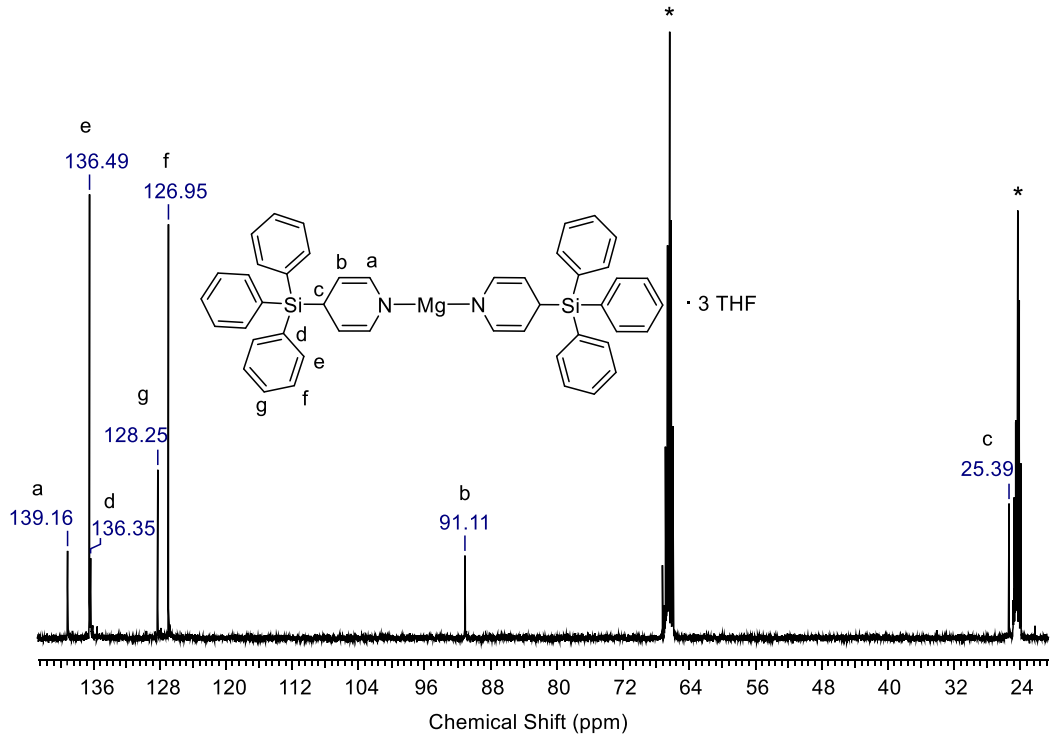

Figure S5. $^{13}C\{^{1}H\}$ NMR spectrum of **2** in THF-d_8 (*) at 25 °C.

2. ^{1}H and $^{13}C\{^{1}H\}$ NMR spectra of $[Mg(NC_5H_6)_2(py)_4]$ (3)

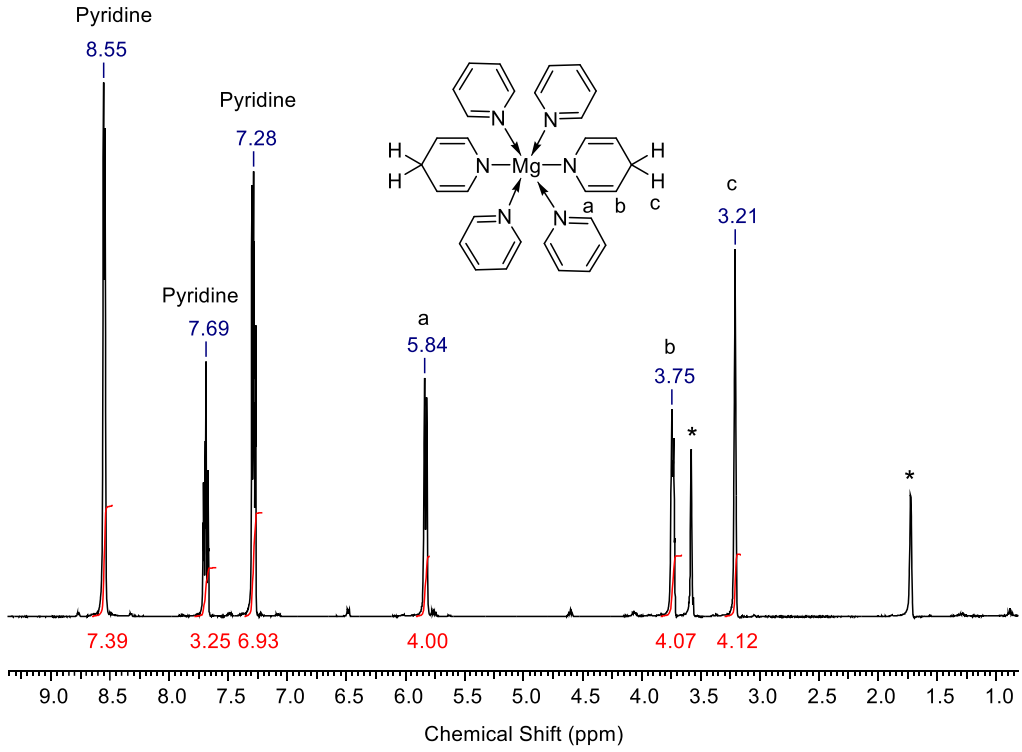

Figure S6. ^{1}H NMR spectrum of **3** in THF-d_8 (*) at 25 °C.

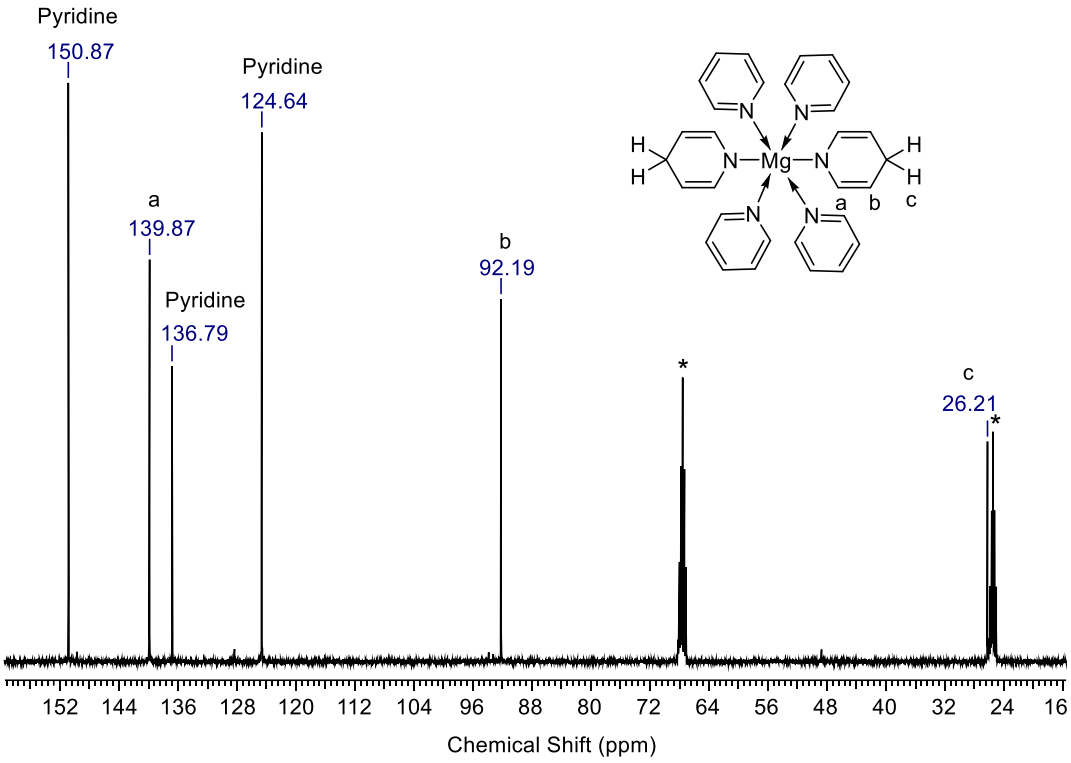

Figure S7. $^{13}C\{^{1}H\}$ NMR spectrum of **3** in THF-d_8 (*) at 25 °C.

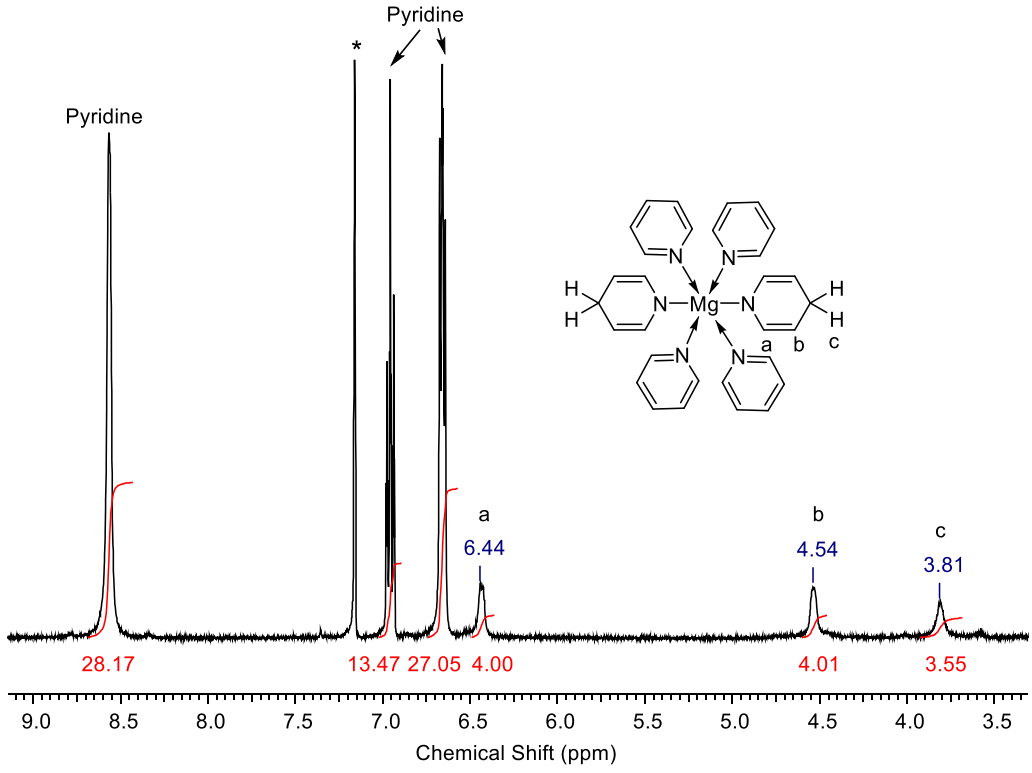

Figure S8. ^{1}H NMR spectrum of **3** in benzene-d_6 (*) at 25 °C.

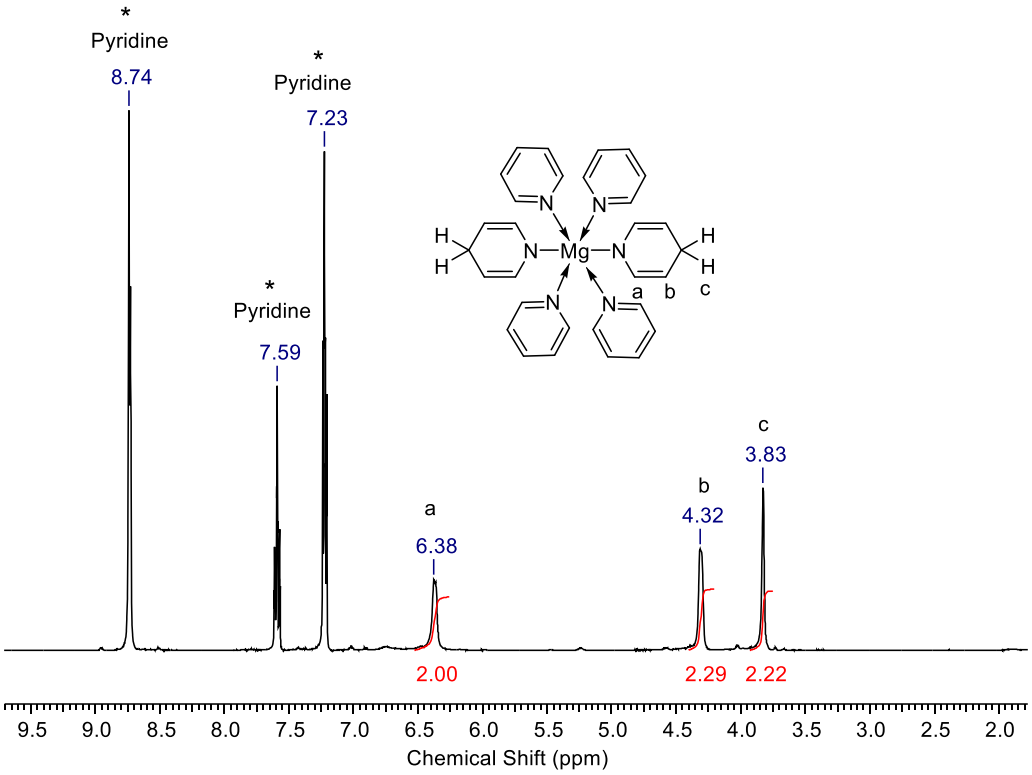

Figure S9. ^{1}H NMR spectrum of **3** in pyridine-d_5 (*) at 25 °C.

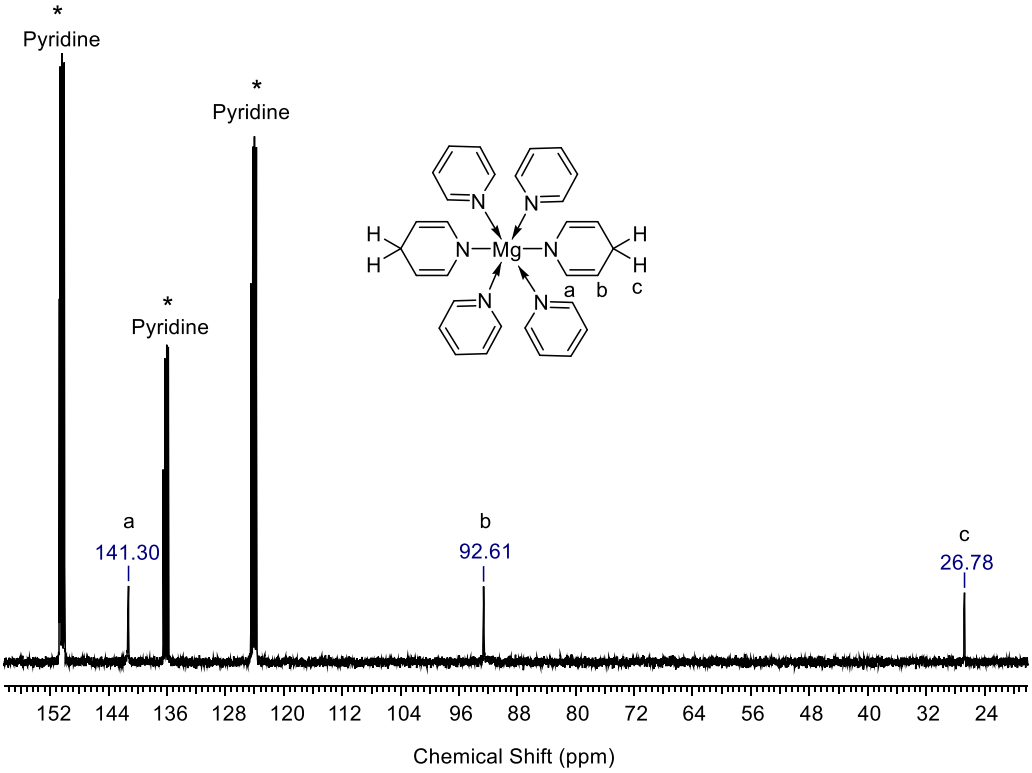

Figure S10. ^{13}C{^{1}H} NMR spectrum of **3** in pyridine-d_5 (*) at 25 °C.

3. ^{1}H and $^{13}C\{^{1}H\}$ NMR spectra of $[Mg(NC_5D_5H)_2(py\text{-}d_5)_4]$ (3-HD)

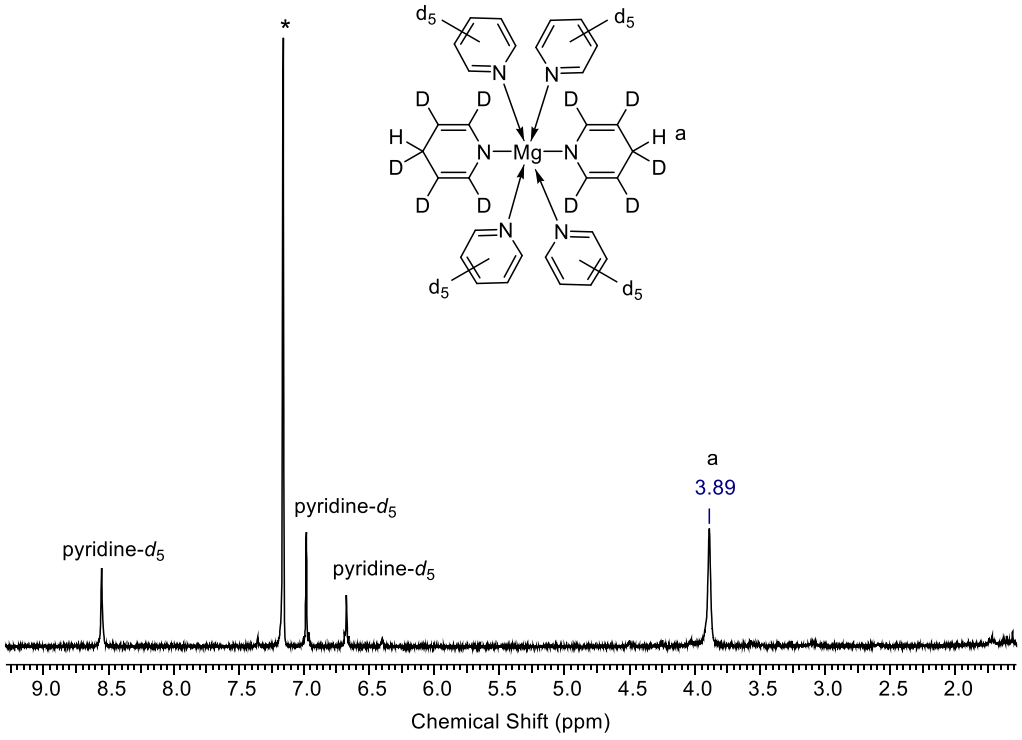

Figure S11. ^{1}H NMR spectrum of **3**-**HD** in benzene-d_6 (*) at 25 °C.

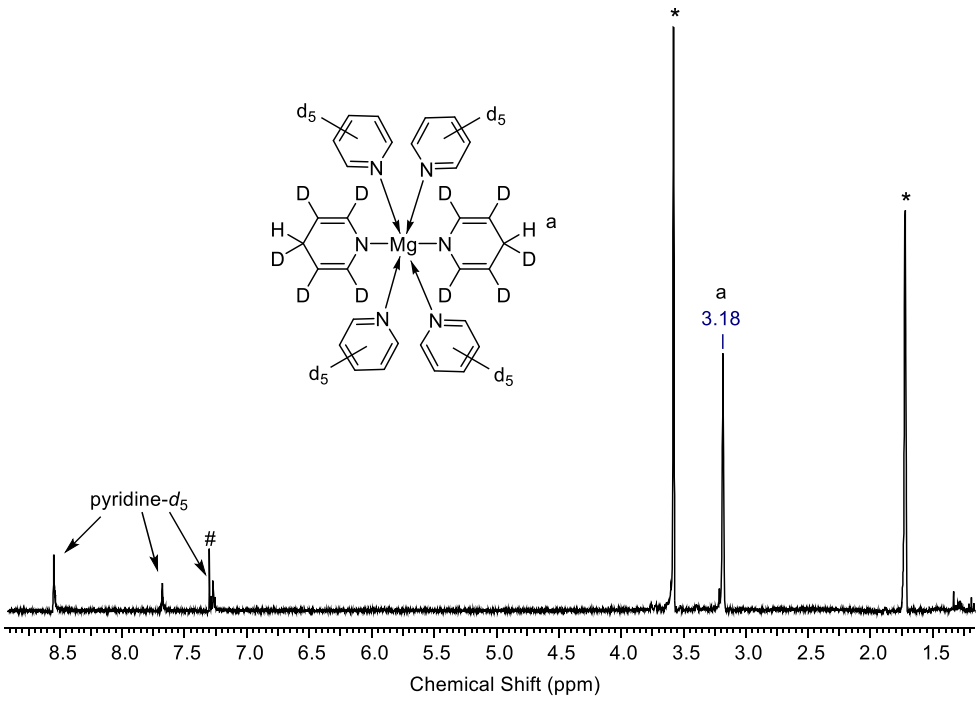

Figure S12. ^{1}H NMR spectrum of **3**-**HD** in THF-d_8 (*) at 25 °C (# unidentified species).

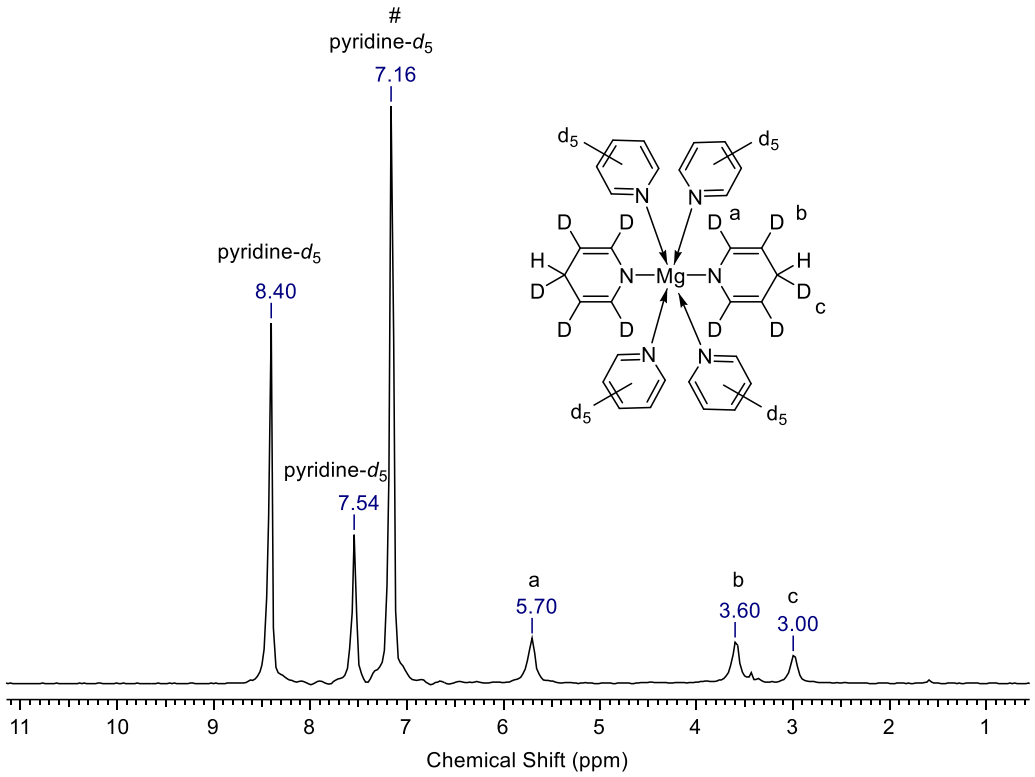

Figure S13. ^{2}D NMR spectrum of **3-HD** in THF with benzene-d_6 as standard (#) at 25 °C.

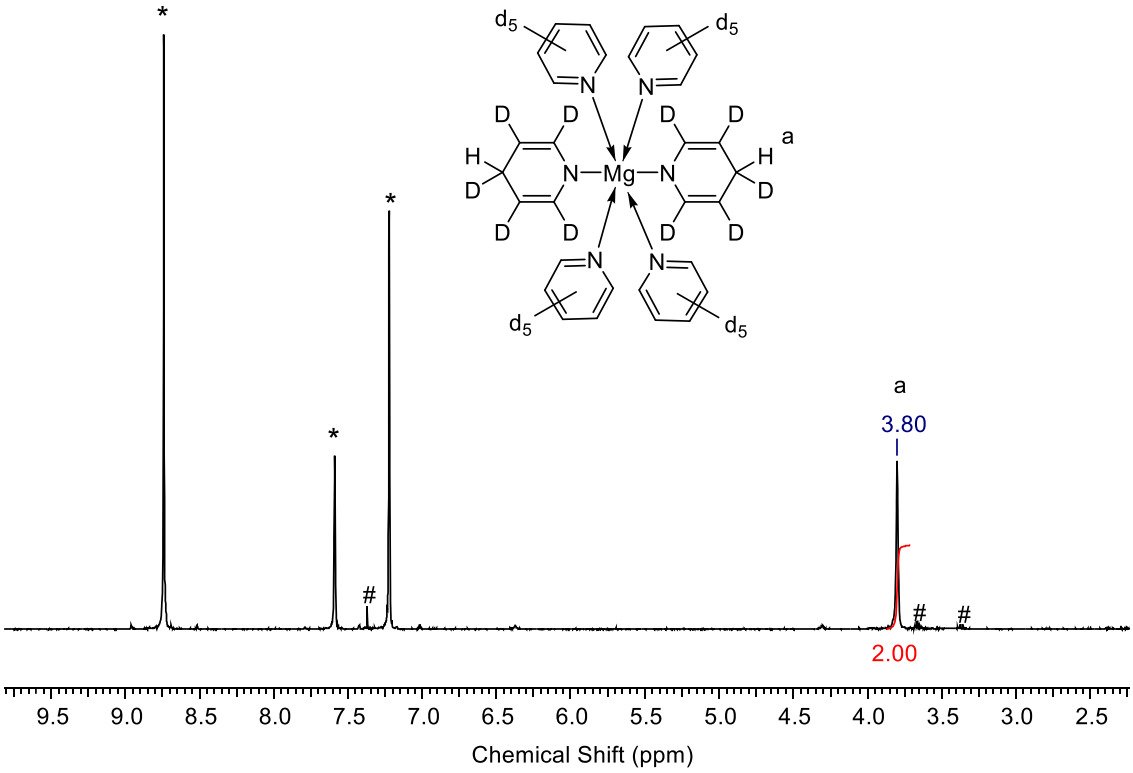

Figure S14. ^{1}H NMR spectrum of **3-HD** in pyridine-d_5 (*) at 25 °C.

4. ^{1}H, $^{13}C\{^{1}H\}$ and $^{29}Si\{^{1}H\}$ NMR spectra of [(Me$_3$TACD)Mg(NC$_5$H$_5$-4-SiPh$_3$)] (5)

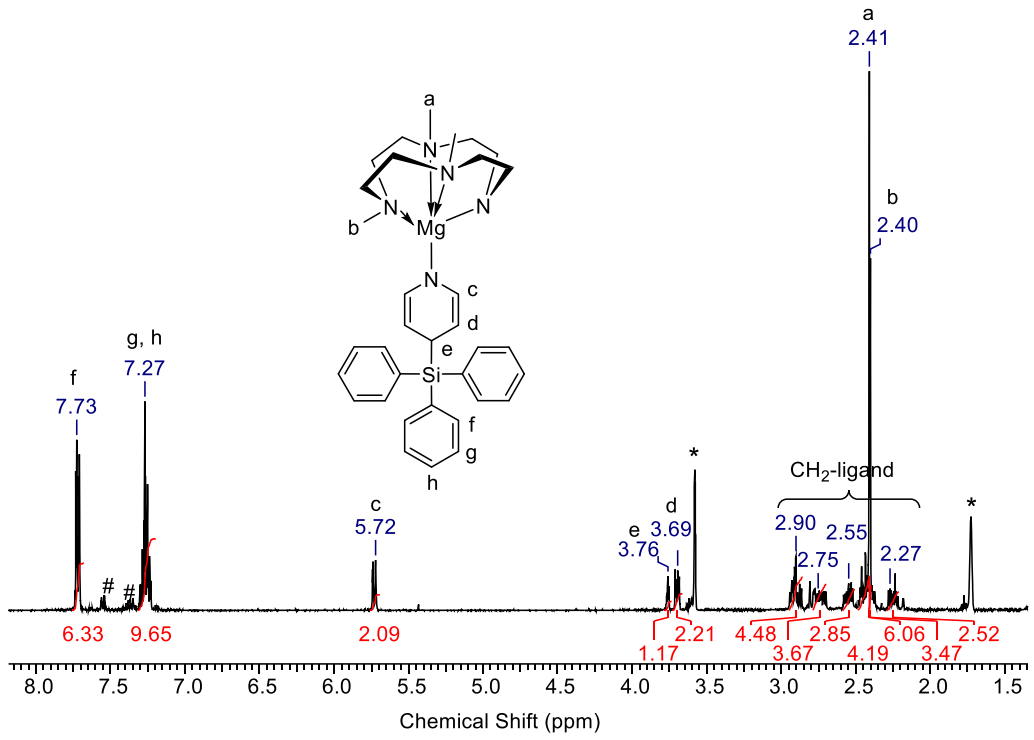

Figure S15. ^{1}H NMR spectrum of **5** in THF-d_8 (*) at 25 °C (# unidentified species).

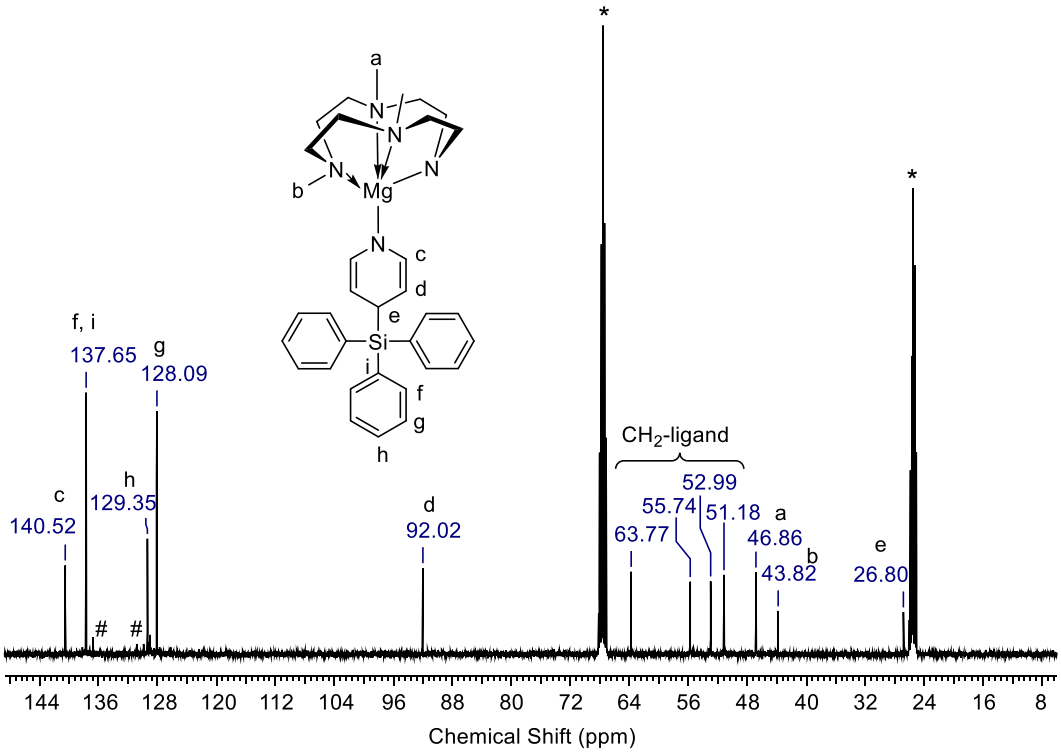

Figure S16. $^{13}C\{^{1}H\}$ NMR spectrum of **5** in THF-d_8 (*) at 25 °C (# unidentified species).

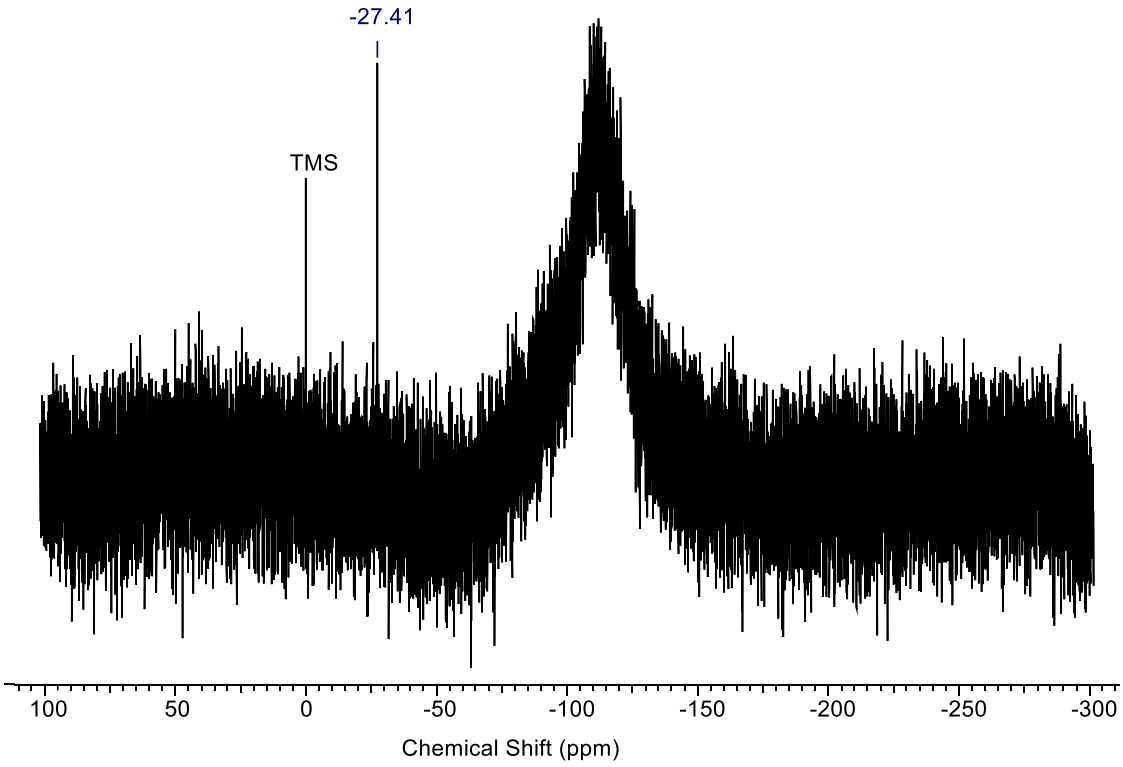

Figure S17. $^{29}Si\{^{1}H\}$ NMR spectrum of **5** in THF-d_8 at 25 °C.

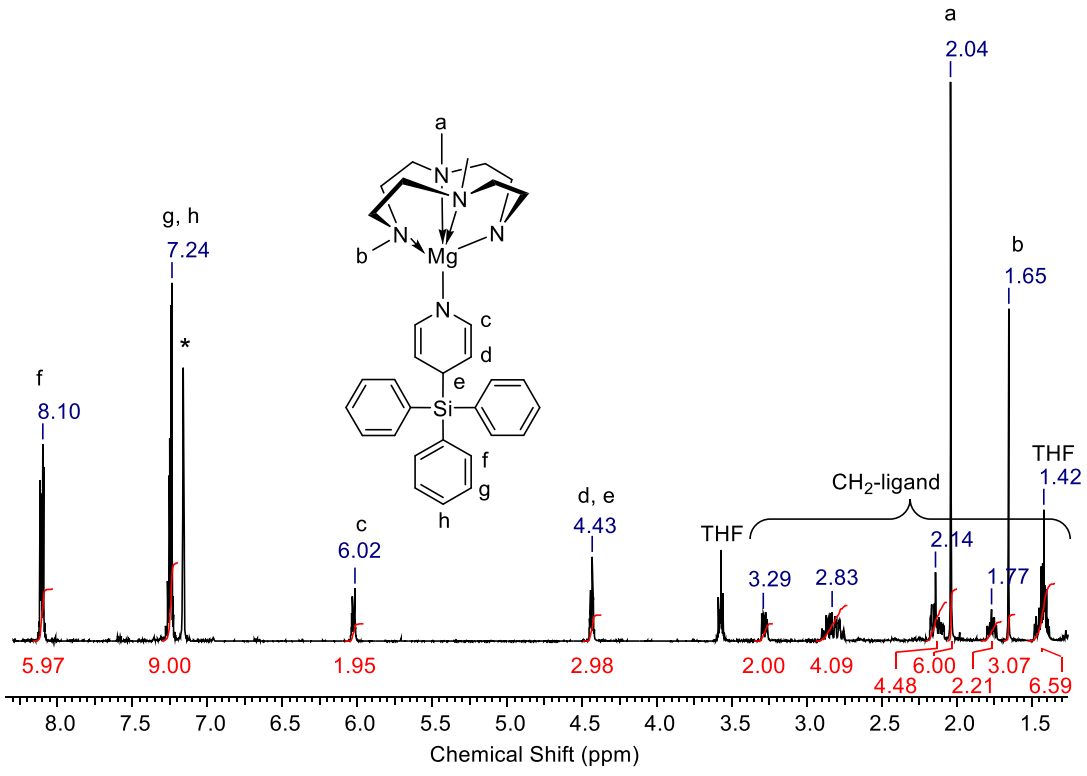

Figure S18. ^{1}H NMR spectrum of **5** in benzene-d_6 (*) at 25 °C.

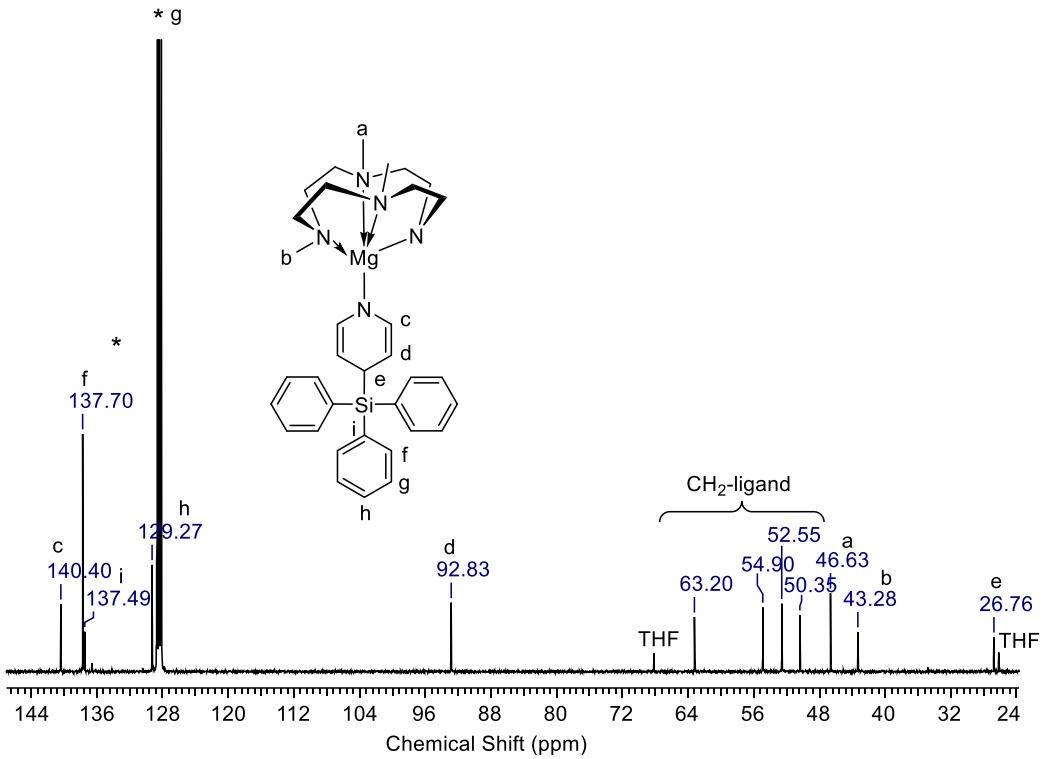

Figure S19. $^{13}C\{^{1}H\}$ NMR spectrum of **5** in benzene-d_6 (*) at 25 °C.

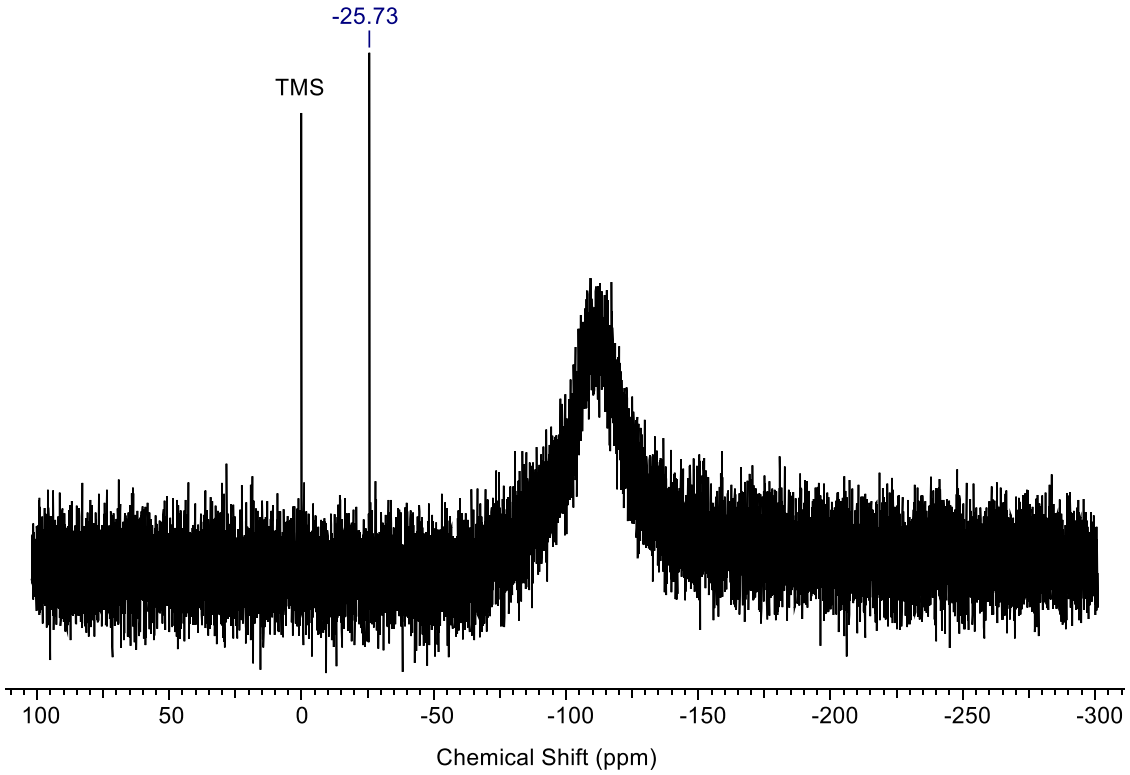

Figure S20. $^{29}Si\{^{1}H\}$ NMR spectrum of **5** in benzene-d_6 at 25 °C.

5. ^{1}H, $^{13}C\{^{1}H\}$ and $^{29}Si\{^{1}H\}$ NMR spectra of [($Me_3TACD{\cdot}AlEt_3$)Mg(NC_5H_5-4-$SiPh_3$)] (7)

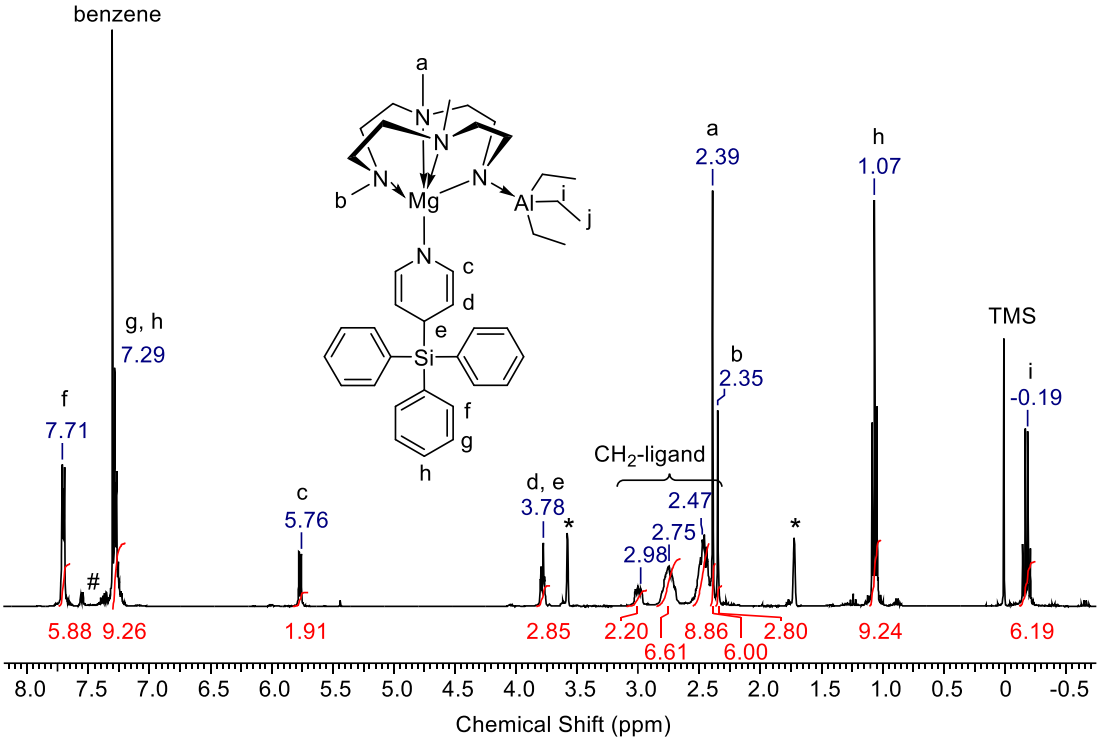

Figure S21. ^{1}H NMR spectrum of **7** in THF-d_8 (*) at 25 °C (# unidentified species).

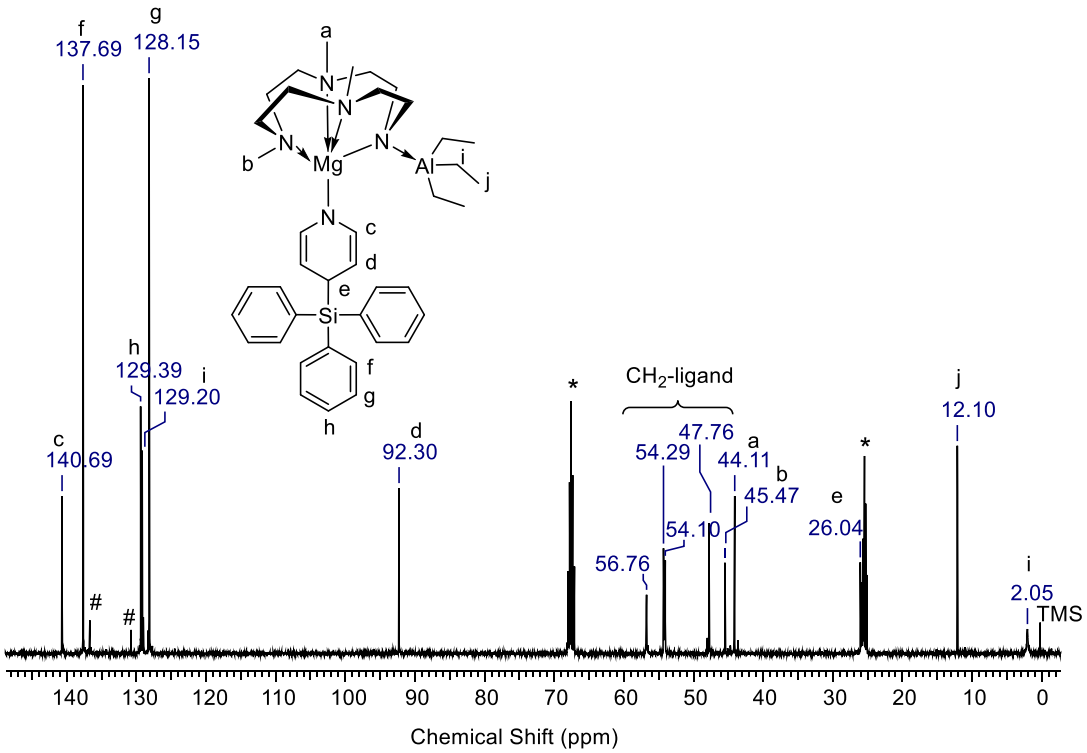

Figure S22. $^{13}C\{^{1}H\}$ NMR spectrum of **7** in THF-d_8 (*) at 25 °C (# unidentified species).

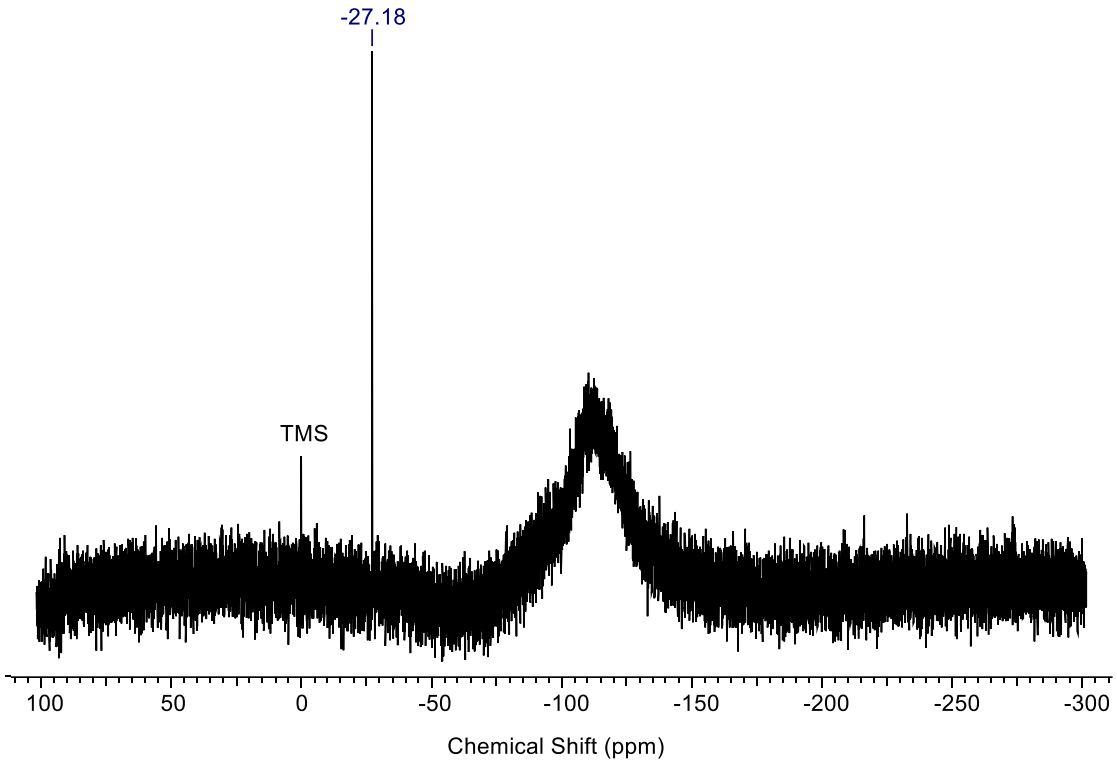

Figure S23. $^{29}Si\{^{1}H\}$ NMR spectrum of **7** in THF-d_8 at 25 °C.

6. ^{1}H and $^{13}C\{^{1}H\}$ NMR spectra of [(Me$_3$TACD)Mg(NC$_5$H$_6$)] (8) + 4-(triphenylsilyl)pyridine

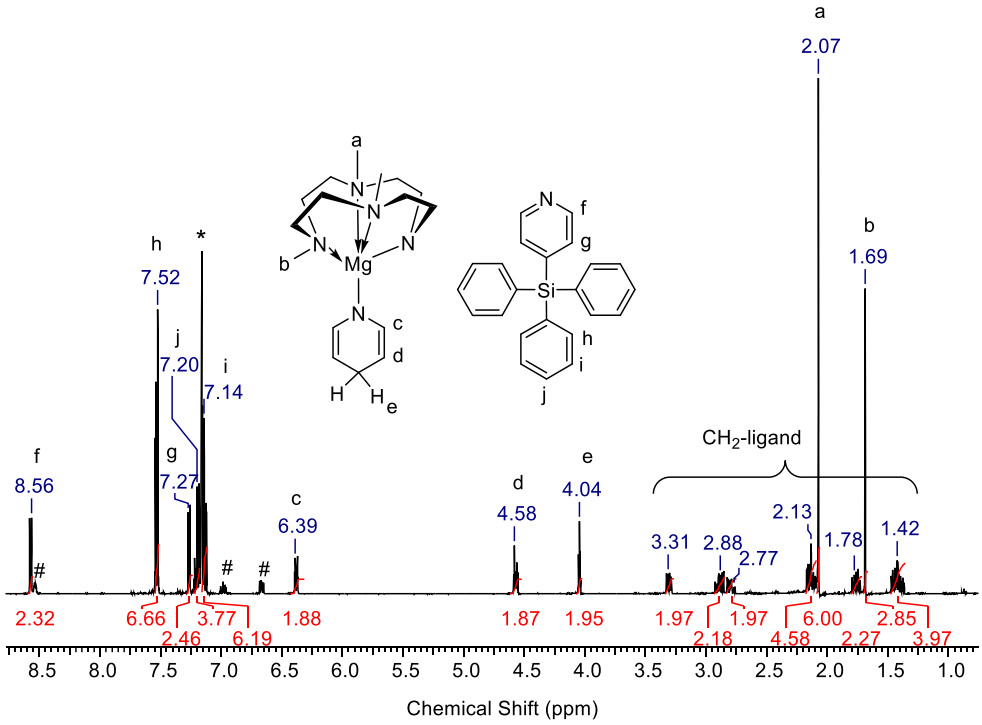

Figure S24. ^{1}H NMR spectrum of **8** and 4-(triphenysilyl)pyridine in benzene-d_6 (*) at 25 °C (# pyridine).

7. ^{1}H and $^{13}C\{^{1}H\}$ NMR spectra of [(Me_3TACD)Mg(NC_5H_6)] (8)

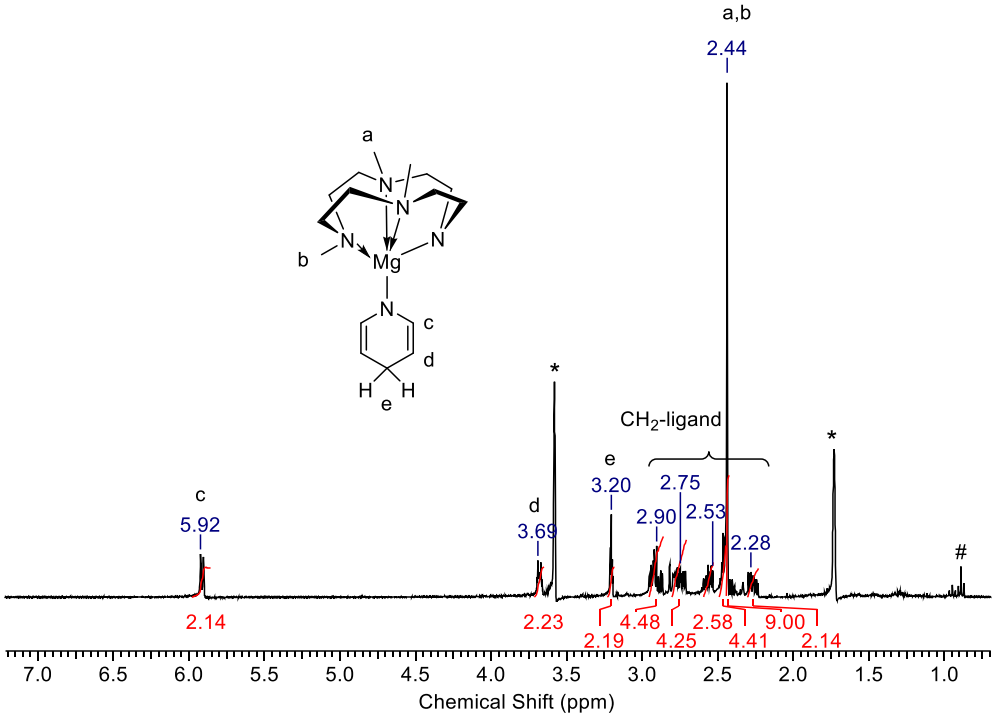

Figure S25. ^{1}H NMR spectrum of **8** in THF-d_8 (*) at 25 °C (# unidentified species).

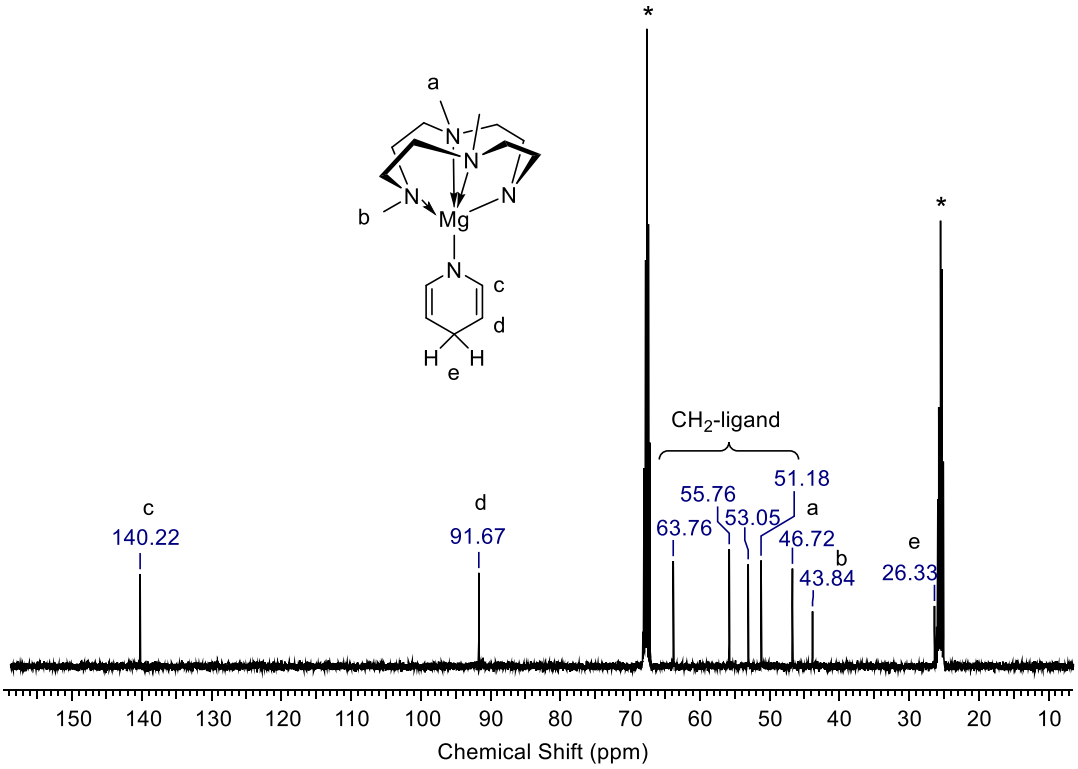

Figure S26. $^{13}C\{^{1}H\}$ NMR spectrum of **8** in THF-d_8 (*) at 25 °C.

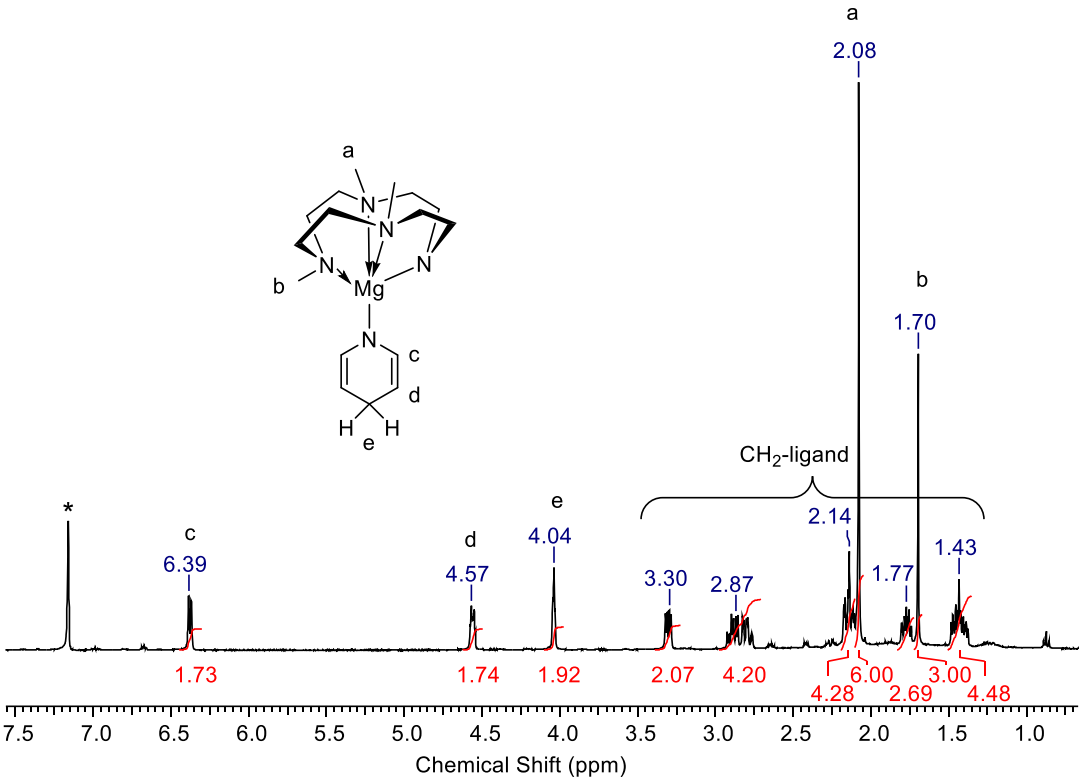

Figure S27. ^{1}H NMR spectrum of **8** in benzene-d_6 (*) at 25 °C.

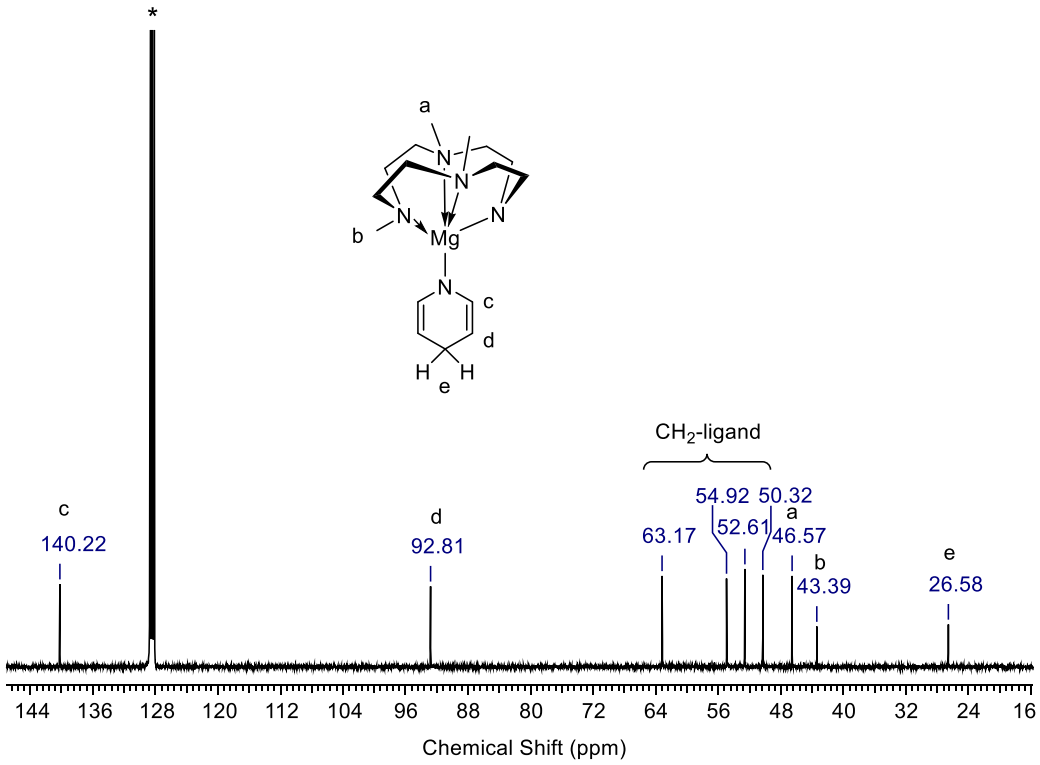

Figure S28. ^{13}C{^{1}H} NMR spectrum of **8** in benzene-d_6 (*) at 25 °C.

8. ^{1}H, $^{13}C\{^{1}H\}$ and $^{29}Si\{^{1}H\}$ NMR spectra of 4-(triphenylsilyl)pyridine

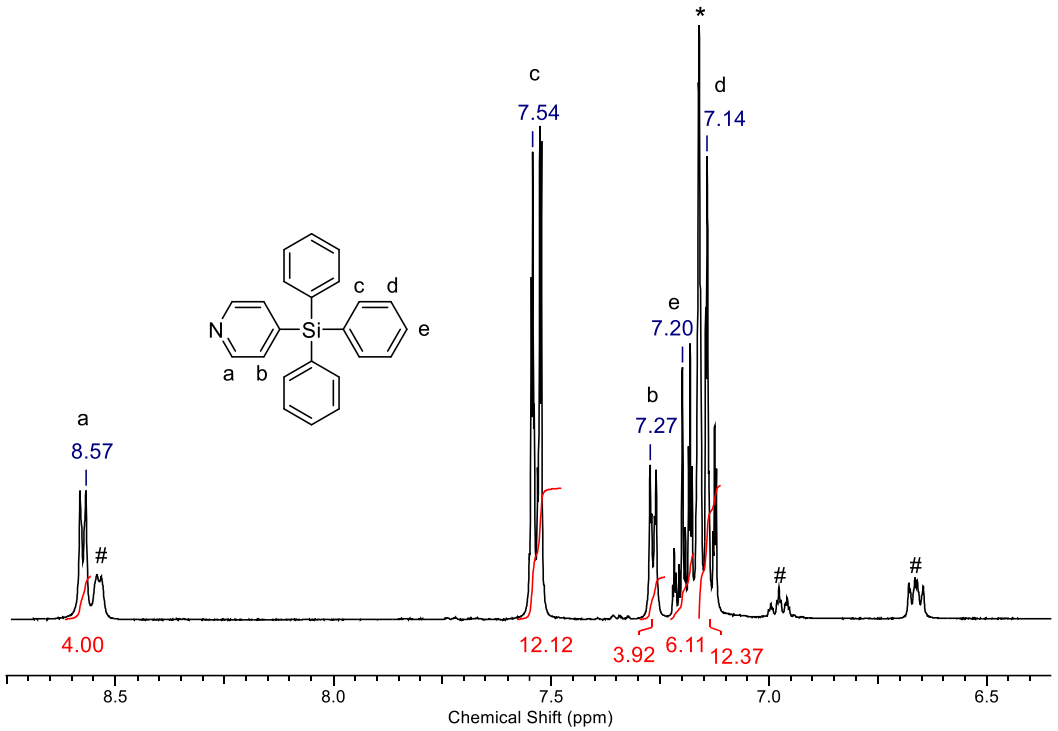

Figure S29. ^{1}H NMR spectrum of 4-(triphenylsilyl)pyridine in benzene-d_6 (*) at 25 °C (# pyridine).

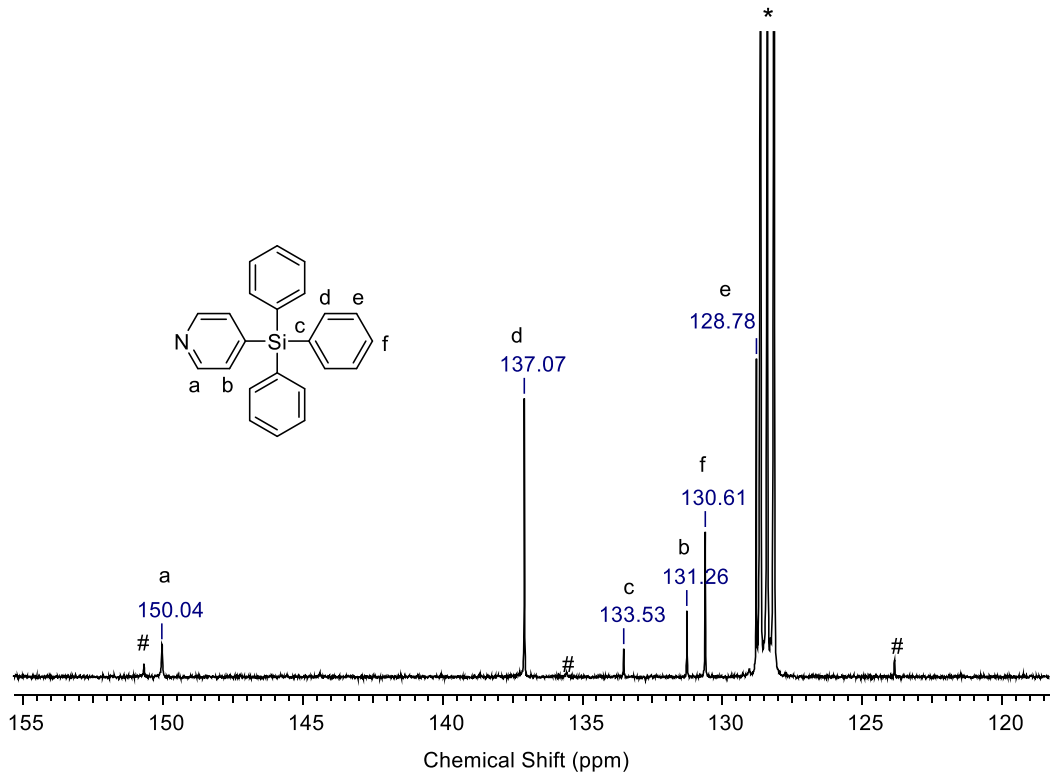

Figure S30. $^{13}C\{^{1}H\}$ NMR spectrum of 4-(triphenylsilyl)pyridine in benzene-d_6 (*) at 25 °C (# pyridine).

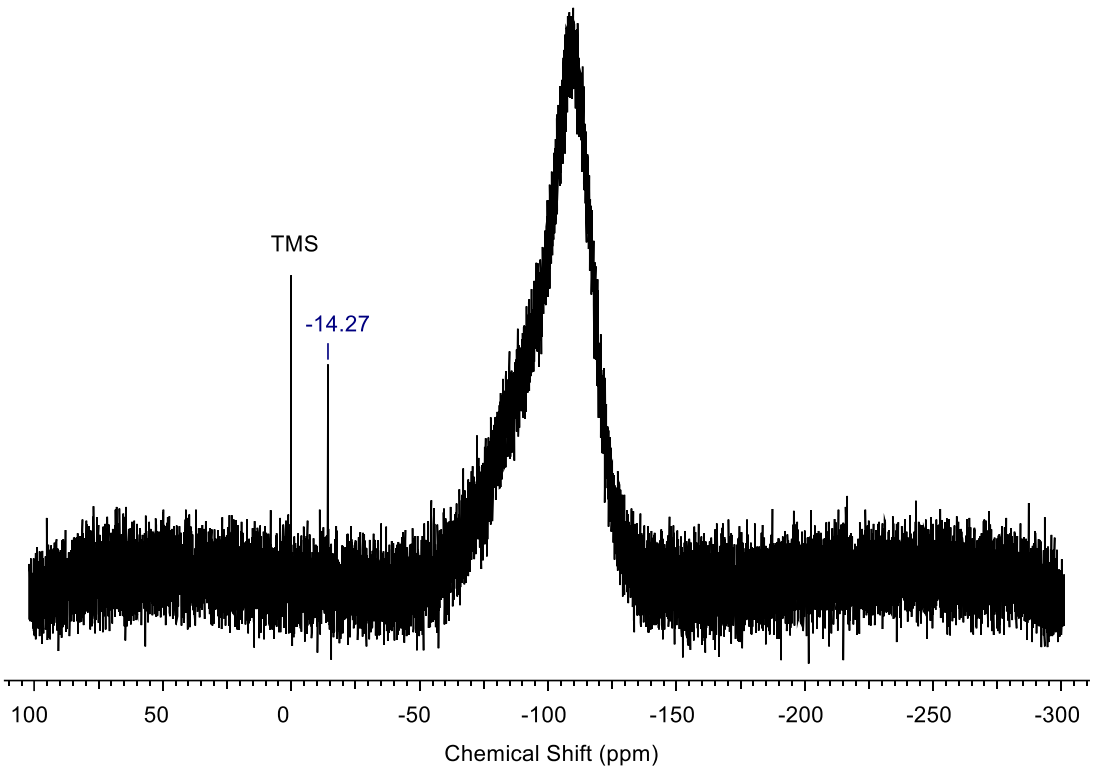

Figure S31. $^{29}Si\{^{1}H\}$ NMR spectrum of 4-(triphenyisilyl)pyridine in benzene-d_6 (*) at 25 °C.

9. Comparison of the ^{1}H NMR signals for the protons of the 1,4-dihydropyridyl ring in 2, 3, 5, 7 and 8

Table S1. Comparison of the ^{1}H NMR signals for the protons of the pyridyl ring in *2*-, *3*- and *4*-position in **2**, **3**, **5**, **7** and **8** in benzene-d_6 and thf-d_8 in ppm.

Complex	Solvent	*2*-Position	*3*-Position	*4*-Position
2	benzene-d_6	5.95	4.56	4.00
	THF-d_8	5.56	3.74	3.81
3	benzene-d_6	6.45	4.54	3.81
	THF-d_8	5.84	3.75	3.21
5	benzene-d_6	6.02	4.43	
	THF-d_8	5.72	3.69	3.76
7	THF-d_8	5.76	3.78	
8	benzene-d_6	6.39	4.57	4.04
	THF-d_8	5.91	3.68	3.20

10. Catalytic hydrosilylation and hydroboration of pyridine

Preparation of a sample for the catalytic hydrosilylation of pyridine.

A J. Young NMR tube was charged with pyridine (24 mg, 24 μL, 0.3 mmol), $PhSiH_3$ (32 mg, 37 μL, 0.3 mmol), hexamethylbenzene (16 mg, 0.1 mmol) and THF-d_8 (0.5 mL) and a ^{1}H NMR spectrum was recorded. After addition of the catalyst (10 mol%), the reaction mixture was heated to 80 °C and the progress of the reaction mixture was monitored by ^{1}H NMR spectroscopy.

Preparation of a sample for the catalytic hydroboration of pyridine.

A J. Young NMR tube was charged with pyridine (24 mg, 24 μL, 0.3 mmol) or 4-*tert*-butylpyridine (41 mg, 44 μL, 0.3 mmol), HBPin (38 mg, 44 μL, 0.3 mmol), hexamethylbenzene (16 mg, 0,1 mmol) and THF-d_8 or benzene-d_6 (0.5 mL) and a ^{1}H NMR spectrum was recorded. After addition of the catalyst (10 mol%), the reaction mixture was heated to 80 °C and the progress of the reaction mixture was monitored by ^{1}H NMR spectroscopy.

Example of a ^{1}H NMR spectrum of the catalytic hydroboration of pyridine.

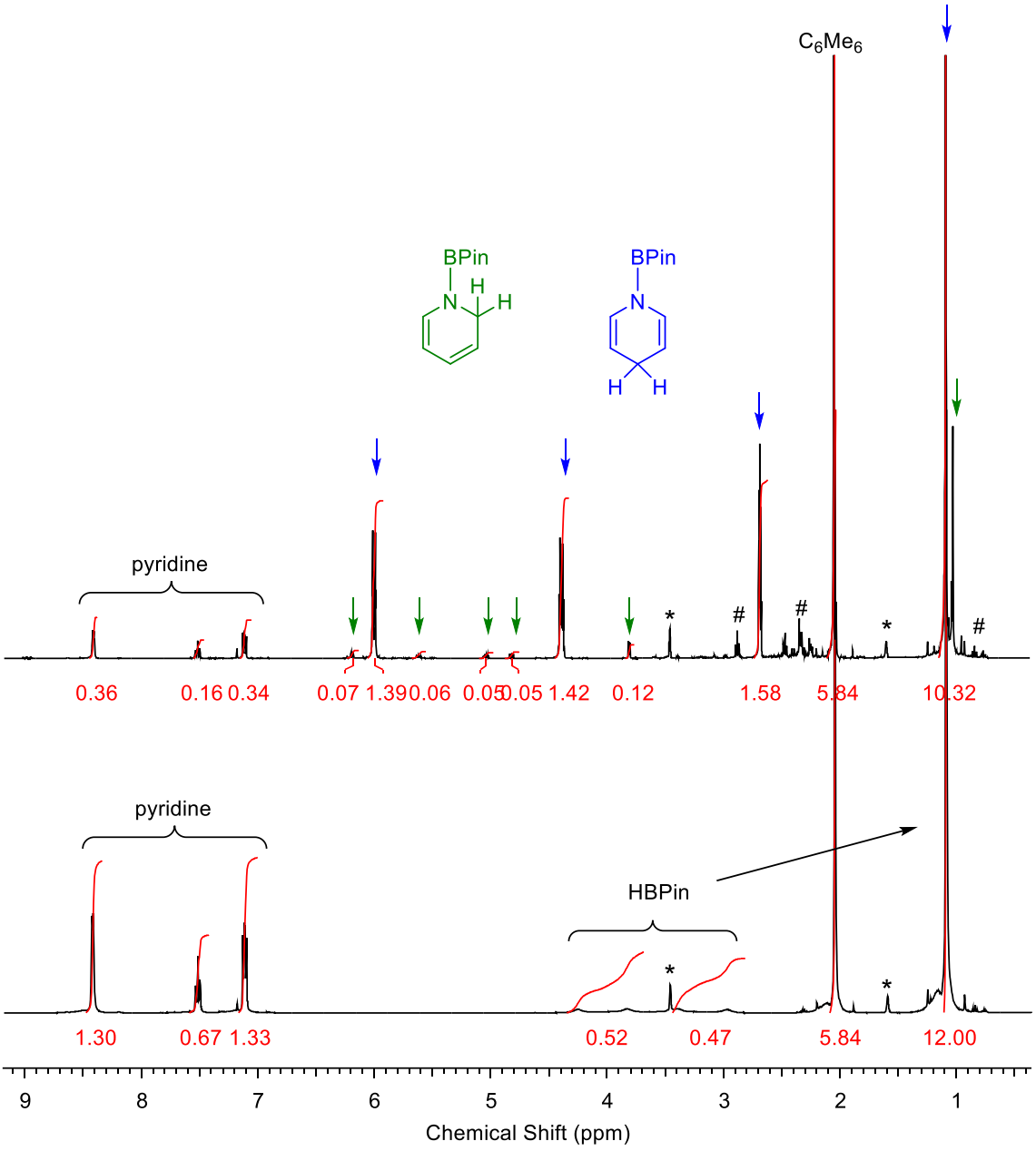

Figure S32. ^{1}H NMR spectra of the catalytic hydroboration of pyridine with pinacolborane (HBPin) in THF-d_8 (*) before adding the catalyst (bottom) and after adding the catalyst and heating for 72 h at 80 °C (top).

11. Exchange of 3 and 8 with pyridine-d_5 to give 3-HD and 8-HD

$[Mg(NC_5H_6)_2(py)_4]$ (**3**) shows an exchange with pyridine-d_5 to give $[Mg(NC_5D_5H)_2(py\text{-}d_5)_4]$ (**3-HD**). The exchange is reversible as **3-HD** reacts with pyridine back to **3** as monitored by ^{1}H NMR spectroscopy in THF-d_8 (Figure S33).

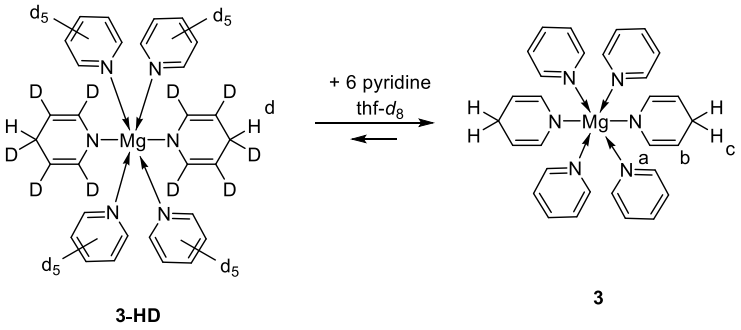

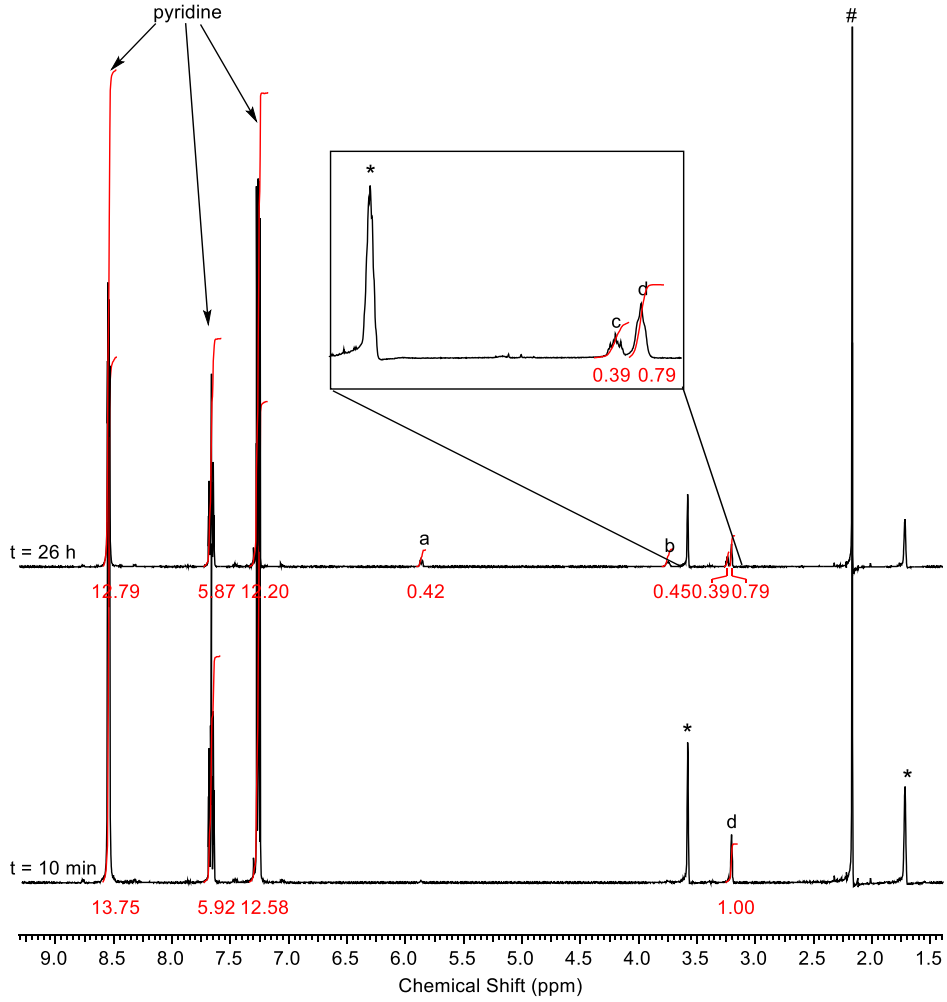

Figure S33. ^{1}H NMR spectra of **3-HD** and 6 equivalents of pyridine in THF-d_8 (*) after 10 min (bottom) and after 26 h at 25 °C (top).

The reaction of **3** with excess pyridine-d_5 to give **3**-**HD** was monitored by ^{1}H NMR spectroscopy at different temperatures. A sample concentration of c = 0.06 mol/L was adjusted by mixing [Mg(NC$_5$H$_6$)$_2$(py)$_4$] (**3**) (15 mg; 0.03 mmol), hexamethylbenzene (internal standard; 2.4 mg; 0.015 mmol) and 0.5 mL of pyridine-d_5. A plot of the amount of **3** versus time at different temperatures is given in Figure S34.

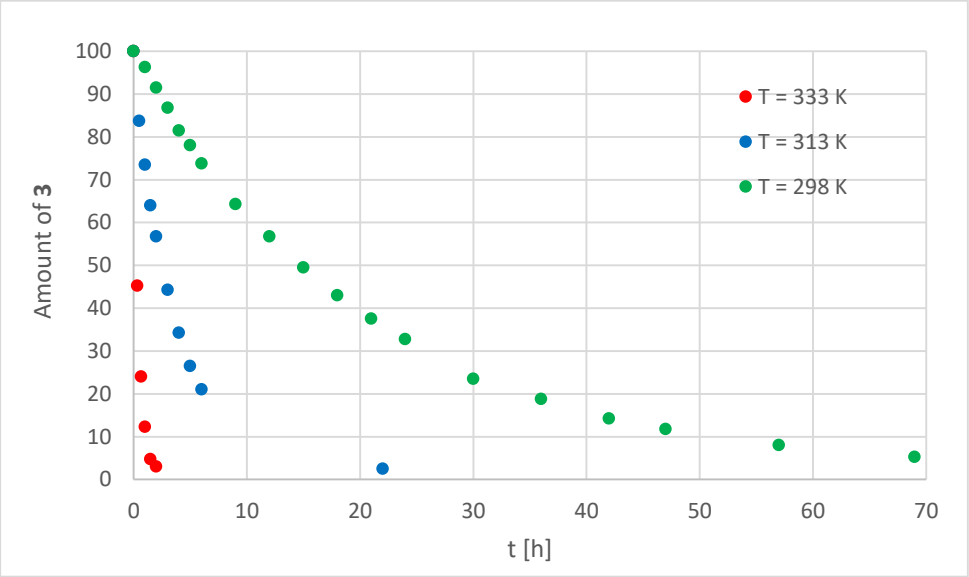

Figure S34. Amount of **3** versus time at at 298 K (green), 313 K (blue) and 333 K (red).

The reversible exchange of **3** in pyridine-d_5 to **3**-**HD** follows pseudo-first order kinetics and can be described by the following equation (Equation S1).

$$[c] = [c_0] \cdot e^{-k_1 \cdot t} \rightarrow \ln([c]/[c_0]) = -k \cdot t$$

Equation S1. First order kinetics.

To determine the reaction rate of the reversible exchange of **3** with excess pyridine-d_5, ln(c(**3**)/c$_0$(**3**)) versus time was plotted for the different temperatures (Figure S35). The slope was deduced from the plot for each temperature (straight lines).

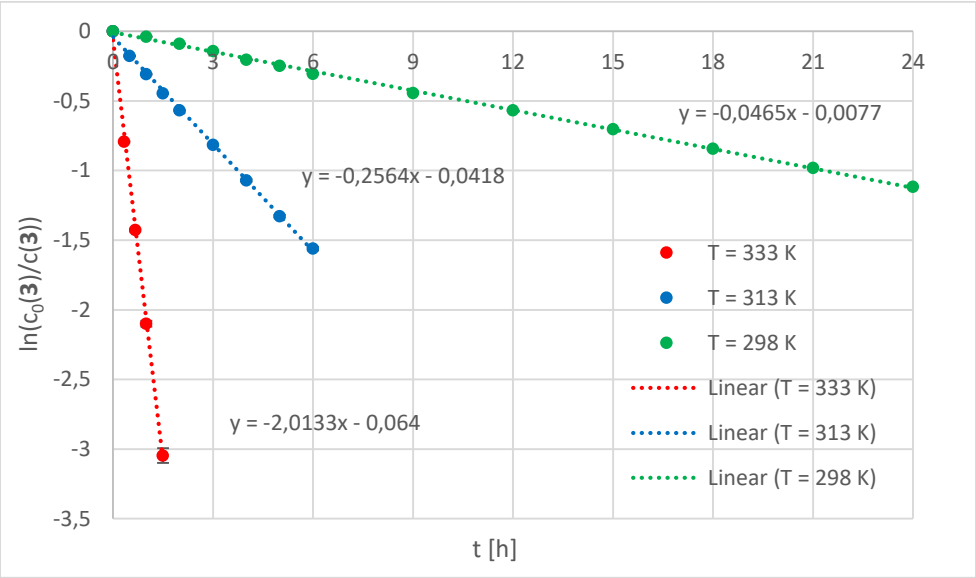

Figure S35. Pot of ln(c(**3**)/c_0(**3**)) versus time for the reaction of **3** with excess pyridine-d_5 at 298 K (green), 313 K (blue) and 333 K (red).

The reaction rates of the reversible exchange of **3** with pyridine-d_5 at different temperatures can be determined from the slope (k_1(298 K) = (1.29±0.01)·10^{-5} s^{-1}, half life $t_{1/2}$ = 15 h; k_1(313 K) = (7.12±0.08)·10^{-5} s^{-1}, half life $t_{1/2}$ = 2.7 h; k_1(333 K) = (5.59±0.10)·10^{-4} s^{-1}, half life $t_{1/2}$ = 0.3 h). The reaction rate is dependent on the temperature and can be described by the Arrhenius equation (Equation S2).

$$k = A \cdot e^{-E_A/R \cdot T} \rightarrow \ln(k) = \ln(A) - \frac{E_A}{R} \cdot \frac{1}{T}$$

Equation S2. Arrhenius equation.

To determine the activation energy E_A of the reversible exchange of **3** with excess pyridine-d_5, ln(k) versus 1/T was plotted for the different temperatures (Figure S36). The slope was deduced from the plot to determine the activation energy (E_A = (70.1±0.6)·kJ·mol^{-1}).

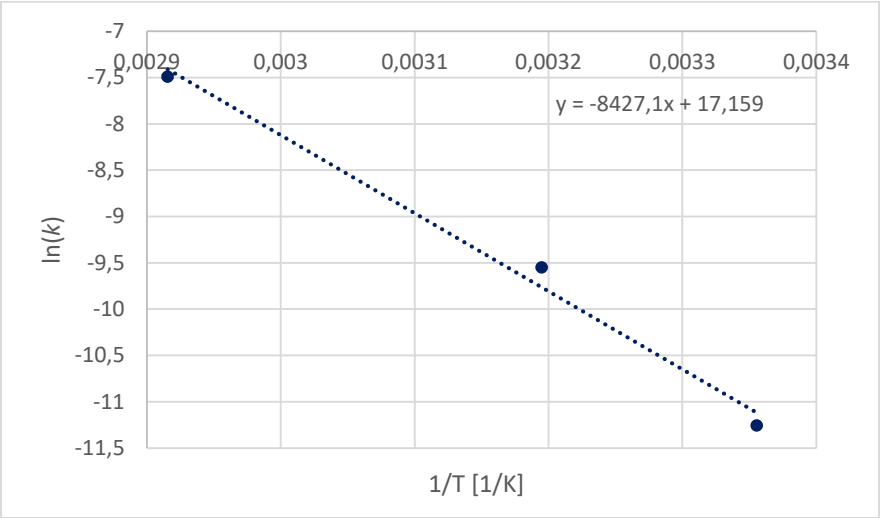

Figure S36. Pot of ln(*k*) versus 1/T for the reaction of **3** with excess pyridine-d_5.

The reaction of **8** with excess pyridine-d_5 to give **8**-**HD** was monitored by ^{1}H NMR spectroscopy at different temperatures. A sample concentration of c = 0.06 mol/L was adjusted by mixing [(Me_3TACD)Mg(NC_5H_6)] (**8**) (9.5 mg; 0.03 mmol), hexamethylbenzene (internal standard; 2.4 mg; 0.015 mmol) and 0.5 mL of pyridine-d_5. A plot of the amount of **8** versus time at different temperatures is given in Figure S37.

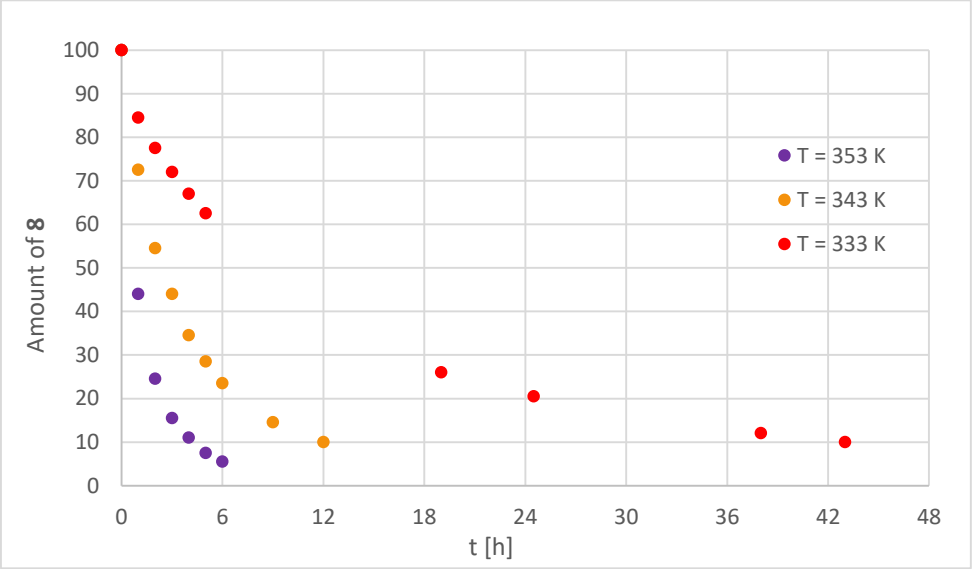

Figure S37. Amount of **8** versus time at 333 K (red), 343 K (orange) and 353 K (purple).

The reversible exchange of **8** in pyridine-d_5 to **8**-**HD** follows pseudo-first order kinetics and can be described by the Equation S1. To determine the reaction rate of the reversible exchange of **8** with excess pyridine-d_5, ln(c(**8**)/c_0(**8**)) versus time was plotted for the different temperatures (Figure S38). The slope was deduced from the plot for each temperature (straight lines).

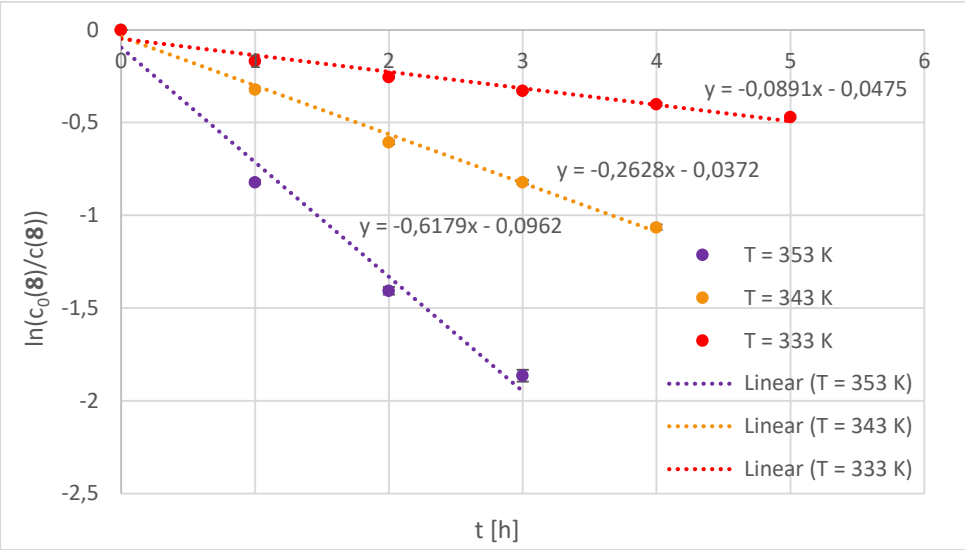

Figure S38. Pot of ln(c(**8**)/c_0(**8**)) versus time for the reaction of **8** with excess pyridine-d_5 at 333 K (red), 343 K (orange) and 353 K (purple).

The reaction rates of the reversible exchange of **8** with pyridine-d_5 at different temperatures can be determined from the slope (k_1(333 K) = (2.48±0.06)·10^{-5} s^{-1}, half life $t_{1/2}$ = 7.8 h; k_1(343 K) = (7.30±0.13)·10^{-5} s^{-1}, half life $t_{1/2}$ = 2.6 h; k_1(353 K) = (1.72±0.02)·10^{-4} s^{-1}, half life $t_{1/2}$ = 1.1 h). The reaction rate is dependent on the temperature and can be described by Equation S2. To determine the activation energy E_A of the reversible exchange of **8** with excess pyridine-d_5, ln(k) versus 1/T was plotted for the different temperatures (Figure S39). The slope was deduced from the plot to determine the activation energy (E_A = (94.7±1.9)·kJ·mol^{-1}).

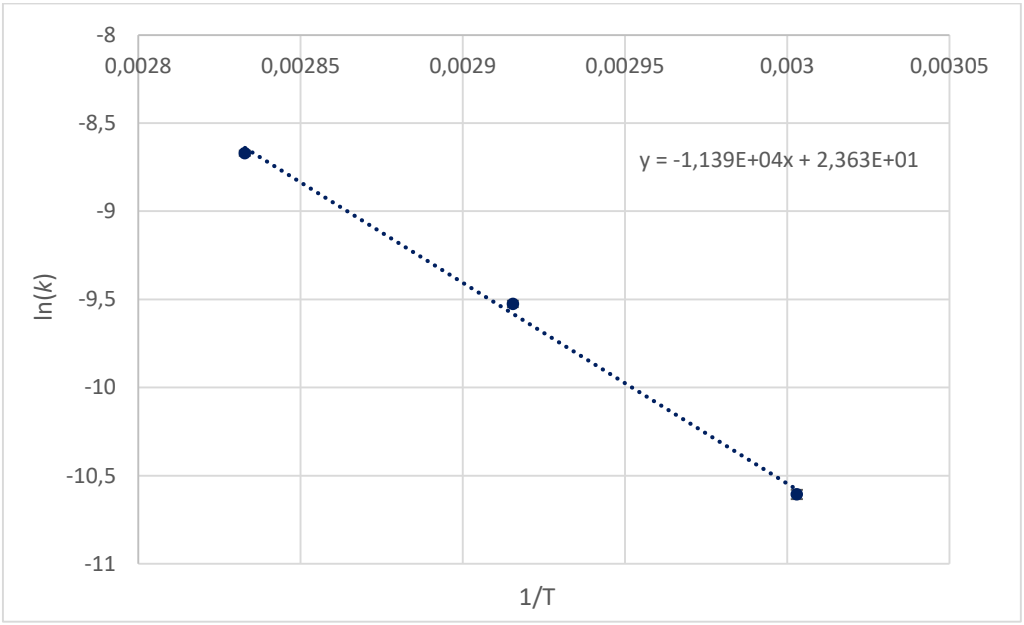

Figure S39. Pot of ln(k) versus 1/T for the reaction of **8** with excess pyridine-d_5.

12. X-ray crystallography

Intensity data for **3** and **5** were collected on a Bruker D8 goniometer with an APEX CCD area-detector and intensity data for **8** were collected on a Eulerian 4-circle diffractometer (STOE STRADIVARI). All measurements were carried out at –173 °C in ω-scan mode. Data reductions and absorption corrections were carried out with the programs SAINT[S1] and SADABS[S2] (**3** and **5**) or with X-Area[S3] and STOE X-Red32[S4] (**8**).

All structures were solved with SIR-92.[S5] **3** contains four crystallographically independent co-crystallized non-coordinated pyridine molecules. Three of them are found around crystallographic symmetry elements (Wyckoff positions 4*e*, 4*c* and 4*d* in space group *I*2/*a*) and show C_i or C_2 symmetry, respectively. The crystallographic symmetry leads to disorder of an N atom against a CH unit (involving N8 and C36, N9 and C40 as well as N10 and C43). The solid of **5** contains one non-coordinated toluene molecule. **5** contains a slightly disordered Me_3TACD fragment which could be resolved well with split positions for the atoms C4, C5, and C10.

All refinements were performed against F^2 with SHELXL-2013[S6] as implemented in the program system WinGX.[S7] All non-hydrogen atoms were assigned anisotropic displacement parameters.

In **3**, all hydrogen atoms of the molecule and of one co-crystallized pyridine molecule were refined in their position. The hydrogen atoms of the three pyridine molecules that are found with crystallographic symmetry and therefore involve disorder are included in calculated positions and were treated as riding in the refinement. In **5**, all hydrogen atoms were included in calculated position and treated as riding, except for hydrogen atom C14 that was refined in its position. All hydrogen atoms in **8** were refined in their position with isotropic displacement parameters.

Graphical representations were performed with the program DIAMOND.[S8]

Table S2. Crystal data and convergence results for compounds **3**, **5** and **8**.

	3	**5**	**8**
formula	$C_{85}H_{89}Mg_2N_{17}$	$C_{41}H_{53}MgN_5Si$	$C_{16}H_{31}MgN_5$
Fw /g·mol^{-1}	1397.35	668.28	317.77
color, habit	orange, rod	yellow block	colorless block
crystal size / mm	0.31 × 0.32 × 0.43	0.09 × 0.12 × 0.16	0.07 × 0.10 × 0.15
crystal system	monoclinic	triclinic	monoclinic
space group	*I*2/*a*	$P\bar{1}$	*I*2/*a*
a / Å	21.864(4)	7.5892(8)	20.2890(15)
b / Å	11.040(2)	14.8942(17)	7.5500(5)
c / Å	32.266(5)	18.236(2)	23.1460(14)
α / °		67.9347(19)	
β / °	101.021(5)	81.964(2)	90.814(5)
γ / °		78.815(2)	
V / Å^3	7645(2)	1869.0(4)	3545.2(4)
Z	4	2	8
d_{calc}/Mg·m^{-3}	1.214	1.188	1.191
μ(MoKα)/mm^{-1}	0.089	0.115	0.105
F(000)	2968	720	1392
θ range / °	1.90 – 28.45	1.49 – 26.62	2.65 – 27.50
index ranges	-29 ≤ h ≤ 29, -14 ≤ k ≤ 14, -43 ≤ l ≤ 43	-9 ≤ h ≤ 9, -18 ≤ k ≤ 18, -22 ≤ l ≤ 22	-26 ≤ h ≤ 24, -9 ≤ k ≤ 9, -26 ≤ l ≤ 30
refln.	52336	23152	27730
indep refl (R_{int})	9582 (0.0621)	7835 (0.0458)	4072 (0.1078)
observed reflns	7626	5784	2689
data/restr/param	9582 / 0 / 617	7835 / 0 / 486	4072 / 0 / 323
R_1, *wR*2 [*I*> 2σ(*I*)]	0.0498, 0.1223	0.0567, 0.1341	0.0585, 0.1362
R_1, *wR*2 (all data)	0.0640, 0.1306	0.0795, 0.1487	0.0973, 0.1570
GooF on F^2	1.037	1.038	1.029
largest diff peak, hole/ e·Å^3	0.400, -0.288	0.790, -0.478	0.312, -0.311
CCDC number	1835299	1835300	1835301

References

S1. Bruker, SAINT-Plus. Bruker AXS Inc.: Madison, Wisconsin, USA, 1999.

S2. Bruker, SADABS. Bruker AXS Inc.: Madison, Wisconsin, USA, 2004.

S3. a) X-Area Pilatus3_SV 1.31.131.0, STOE, 2017; b) X-Area Recipe 1.33.0.0, STOE, 2015; c) X-Area Integrate 1.71.0.0, STOE, 2016; X-Area LANA 1.71.4.0, STOE, 2017.

S4. STOE X-Red32, absorption correction by Gaussian integration, analogous to P. Coppens, *The Evaluation of Absorption and Extinction in Single-Crystal Structure Analysis*, published in: F. R. Ahmed (Ed.), *Crystallographic Computing*, Munksgaard, Copenhagen 1970, 255-270.

S5. A. Altomare, G. Cascarano, C. Giacovazzo, A. Guagliardi, *J. Appl. Crystallogr.*, 1993, **26**, 343-350.

S6. G. M. Sheldrick, *Acta Crystallogr., Sect. A*, 2008, **64**, 112-122.

S7. L. J. Farrugia, *J. Appl. Crystallogr.*, 2012, **45**, 849-854.

S8. K. Brandenburg, DIAMOND. Crystal Impact GbR: Bonn, Germany, 2017.